

Validation of SAFIR[®] through DIN EN 1992-1-2 NA

Comparison of the results for the examples
presented in Annex CC

March 2018

J. Ferreira
J.-M. Franssen
T. Gernay
A. Gamba

Table of contents

1.	Introduction	3
1.1.	Form of validation.....	3
1.2.	Structure of the document.....	3
1.3.	Sources of differences in results	3
1.4.	Results versus visualisation.....	4
1.5.	Versions of the software used.....	6
2.	Validation examples.....	7
2.1.	Example 1 – Heat transfer (cooling) with constant properties.....	7
2.2.	Example 2 – Heat transfer (heating) with varying properties	19
2.3.	Example 3 – Heat transfer through several layers	28
2.4.	Example 4 – Thermal expansion.....	31
2.5.	Example 5 – Temperature-dependent stress-strain curves of concrete and steel 37	
2.6.	Example 6 – Temperature-dependent limit-load-bearing capacity of concrete and steel 40	
2.7.	Example 7 – Development of restraint stresses	42
2.8.	Example 8 – Weakly reinforced concrete beam	44
2.9.	Example 9 – Heavily reinforced concrete beam	52
2.10.	Example 10 – Reinforced concrete beam-column	58
2.11.	Example 11 – Composite column with concrete cores.....	64
3.	General conclusions	68
4.	References.....	69

1. Introduction

1.1. Form of validation

Annex CC of DIN EN 1992-1-2 NA [2] presents a series of cases that allow benchmarking software tools aimed at the design of structures in a fire situation.

With the goal of providing a validation document for the finite element code SAFIR [1], a comparison of the reference results for the cases presented in the Annex CC with the results obtained by SAFIR has been carried out and is presented in this document.

The validation typically consists in a comparison between the value of a result (temperature, displacement or others) obtained by SAFIR and the value given as a reference and supposed to be the « *true* » result. The value obtained must fall in the interval stipulated by the document.

1.2. Structure of the document

This document contains comparisons of SAFIR with the examples provided by the DIN. For each example, keywords are initially provided in order to easily detect what is being analysed in the example. The objective of the example is then summarized and a description of the necessary information concerning geometry, boundary conditions, loads, parameters, material laws, etc, is given. Finally, a description of the model used and possible assumptions is presented and the main conclusions about the comparisons of SAFIR to the reference solutions are exposed.

All the SAFIR files used are made available with this document, and references to the folders where they are located are given in the sub-chapters related to each model. The pictures that allow visualizing the results of SAFIR were made with the post-processor DIAMOND 2016, which can be downloaded for free on the SAFIR website.

1.3. Sources of differences in results

Some differences between the results of SAFIR and the reference values may be observed either due to different formulations being used or to the way the results are obtained and presented. This is discussed in the next two sections.

1.3.1 *Significant digits*

In many cases, the true value is a real number and its expression should involve an infinite number of significant digits, like for instance 0,03458623579841265895123548... However, the determined value is always given with a certain resolution, i.e. a limited number of significant digits, and it is not always mentioned whether this has been obtained by rounding or by truncating the true value. In the example above, with only 2 significant digits, the rounded value is 0,035 whereas the truncated value is 0,034¹. Such an uncertainty of 0,001 represents 2,857% of the rounded value and 2,941% of the truncated value whereas the maximum allowed deviation may be as low as 1%.

Moreover, the results produced by SAFIR have by default a limited number of significant digits (typically 8 or 16 digits). As it may not be relevant to print all results with such a high

¹ This reference value of 0,034 is present in Example 5 of DIN EN 1992-1-2.

resolution, results are usually rounded before they are written in the two different files that are produced by SAFIR: *filename.out* and *filename.xml*. In these two files, the resolution may not be the same. For example, the displacements written in the *out* file, meant to be read by the human eye, are in 1/100 of a mm, which is supposed to be sufficiently small for a civil engineering structure. In the *xml* file, however, meant to be used by the graphic postprocessor Diamond, they are written with 3 significant digits.

In the exercises reported in this document, the values considered for SAFIR are always the most precise of both, based on the fact that any user has access to both files. For example, if the example above is a displacement in mm, SAFIR would write 0,00003 in the *out* file and 3,46E-03 in the *xml* file and the later would be used to calculate the deviation from the reference value. In this case, the double effect of rounding or truncating the reference value and of rounding the result of SAFIR would give a deviation of 1,14% with the rounded reference value and 1,76% with the truncated reference value, even if SAFIR calculates the true value to the 8th or 16th significant digit.

In some cases, it is possible to modify the size of the structure to be analysed in the reference case to obtain, at least, more significant digits in the *out* file produced by SAFIR. For example, the thermal expansion of a bar would be 10 times higher if the size of the bar is multiplied by 10. Interested users may want to do that, but this has not been done for this document.

1.3.2 Refinement of the model

The results calculated by a finite element software highly depend on the discretisation of the model in space, with finer grids yielding more correct results. If the analysis is transient, the results also depend on the discretisation in time, with smaller time steps yielding more correct results. The question of the discretisation to be used by the software, to produce the results that will be compared with the reference value, is typically not discussed in the documents that give the reference value.

In this exercise, the results are first presented with a model that is sufficiently refined (in space and in time) to ensure a converged solution, which means that the solution would not be different² with a finer model. Yet, it is highly valuable for the user to have an idea of the convergence of the solution when the model is “degraded”. This allows answering the following question: what level of refinement is required for the software to yield acceptable results? This is why for some of the examples, in addition to the results produced with the converged model, we will present also results obtained with different levels of refinement. It must then come as no surprise if, when the model is too crude, the results don’t fall within the acceptable limits anymore.

1.4. Results versus visualisation

Results produced by SAFIR come in the form of numbers. In order to validate the software, these numbers are considered and compared to the reference values and the results of the comparisons are usually given in tables. Yet, in order to give a more intuitive feeling of the results, these results can also be processed in order to create drawings. The graphical tool DIAMOND has

² Within the limits of the available resolution

been specifically developed at Liege University to create drawings based on SAFIR results and has been used in this report³.

It has yet to be understood that some simplifications may be used to produce the drawings and these are discussed in this section.

1.4.1 Temperature field on triangular facets.

The temperature distribution on a triangular facet of a 3D SOLID element or on a triangular 2D SOLID element varies linearly. The graphic representation of the temperature distribution on such facets being linear is the exact representation of the temperature distribution considered in SAFIR, see Figure 12 for example.

The same holds for the representation of the warping function calculated for a torsion analysis.

1.4.2 Temperature field on quadrangular facets.

The temperature distribution on a quadrangular facet of a 3D SOLID element or on a quadrangular 2D SOLID element varies in a nonlinear manner. Being based on the temperature of the 4 nodes located at the corners of the facet, the temperature distribution is driven by an equation of the type given hereafter.

$$T(x,y) = k_1 + k_2 x + k_3 y + k_4 xy$$

In order to accelerate the drawings, this nonlinear distribution is simplified in DIAMOND. The temperature at the centre of gravity of the facet T_c is calculated exactly as the average of the 4 corner temperatures. Then DIAMOND divides the quadrangle into 4 triangles, each one based on the centre of the quadrangle and 2 adjacent corner nodes, see Figure 1. A linear temperature distribution is then assumed and drawn in each of the 4 triangles, and this distribution is different from the real distribution considered in SAFIR. This effect of artificial linearization is clearly visible, for example, on Figure 30 a) and Figure 31 a).

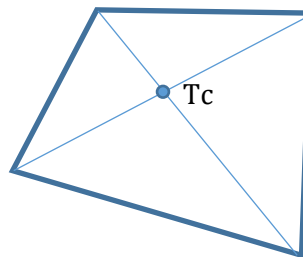


Figure 1 – Division of a quadrangle by DIAMOND

The same holds for the representation of the warping function calculated for a torsion analysis.

The visual effect of the approximation vanishes with the refinement of the mesh.

³ Any other graphical software could be used provided it can read the XML file produced by SAFIR.

1.4.3 Representation of deformed beam elements

Beam finite elements in the deformed configuration are curved, because the end nodes are subjected to a rotation with respect to the chord that joints them. Yet, in order to simplify and to accelerate the drawing process, DIAMOND will draw each beam finite element as a straight line between the end nodes. Here again, the drawn situation does not correspond exactly to the situation considered in SAFIR.

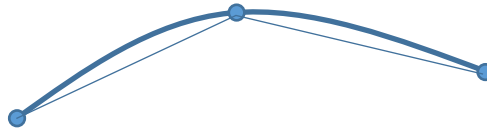


Figure 2 – Simplification of the drawn deformed configurations

In Figure 2, the thick curved line represents schematically a deformed configuration that could be considered by SAFIR whereas the two thin lines represent the configuration that would be drawn by DIAMOND for two beam finite elements.

Here also, the visual effect of the approximation vanishes with the refinement of the mesh.

1.5. Versions of the software used

The version of SAFIR used for performing the calculations was SAFIR 2016.c.0, whereas two different versions of DIAMOND2016 - versions v1.2.1.20 and v1.3.0.0 - were used for visualising the results and creating some of the illustrations presented in this document.

2. Validation examples

2.1. Example 1 – Heat transfer (cooling) with constant properties

2.1.1 Keywords

Heat-transfer, conduction, convection, constant thermal properties

2.1.2 Objective

The goal of this example is to analyse the heat transfer by conduction and convection in a 2D square section with constant thermal properties.

2.1.3 Description of the problem

A square section with the characteristics defined in Figure 1 and Table 1 is analysed. The temperature in the square section is uniform and equal to 1000°C at time $t = 0$ s when it is exposed to a gas with temperature = 0°C on one of the edges, the other edges being adiabatic. Heat transfer from the gas to the solid is by linear convection. In order to validate the results, the temperature θ_0 calculated at the centre of the opposite edge, at point X, is compared to the reference values presented in DIN EN1992-1-2 NA at different time instants.

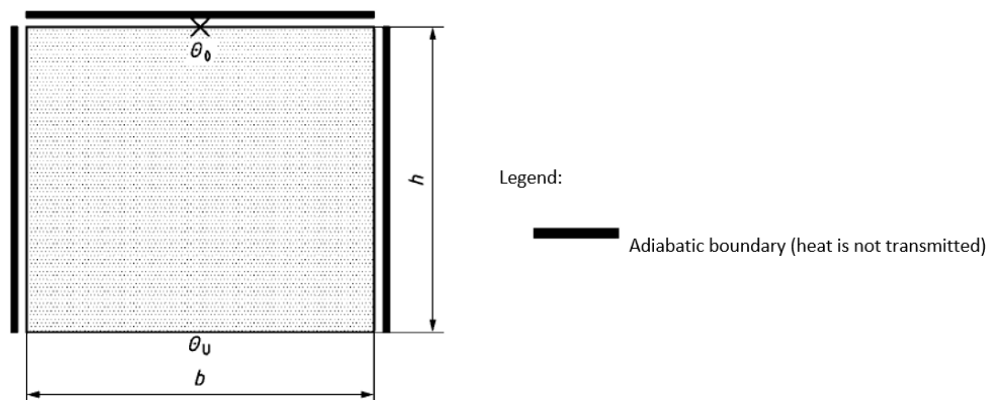


Figure 3 – Example 1: Cooling down process in section with constant properties

Table 1 – Dimensions, material properties and boundary conditions for Example 1

Properties		Value
Thermal conductivity λ	W / (m·K)	1
Specific heat c_p	J / (kg·K)	1
Density ρ	Kg / m ³	1000
Dimensions h, b	M	1
Coefficient of convection α_c	W / (m ² ·K)	1
Emissivity $\epsilon_{res} = \epsilon_m \cdot \epsilon_f$	-	0
Ambient temperature θ_u	°C	0
Temperature in the cross-section θ_{cs}	°C	1000

2.1.4 Model and results (see folder DIN1_4)

As the heat flow is uniaxial, from the exposed edge to the opposite edge, a model with only two rectangular elements on the width of the section is sufficient (in fact, a model with one single element on the width would yield the same answer, but it would not be possible to calculate the temperature at the centre node of the opposite edge). A structured mesh formed by 100 quadrilateral elements was used with 50 elements on the height, as depicted in Figure 4. Each of these elements contains 4 gauss points of integration (2x2) in its plane.

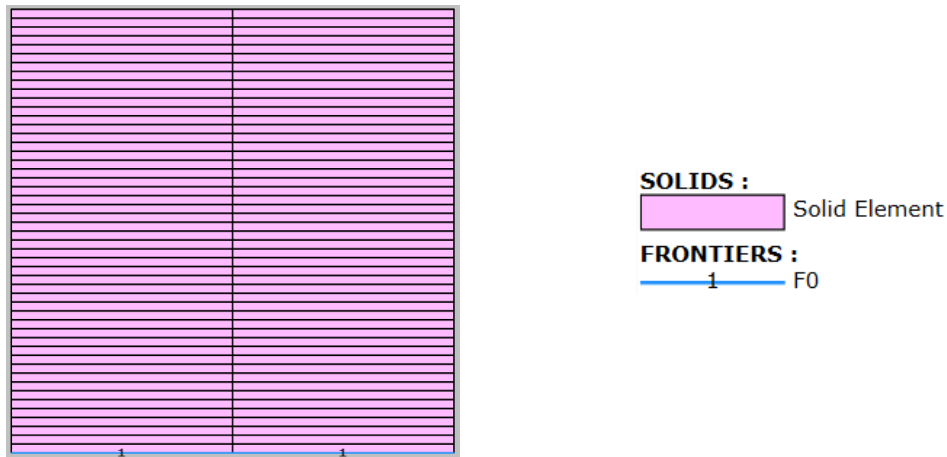


Figure 4 – Thermal model of the cross-section for Example 1 (2 x 50 SOLID elements)

In SAFIR, a FRONTIER constraint with the function F0 was applied on the exposed edge, i.e. the lower edge in Figure 4 .

The PRECISION command was set to 1.0E-3. The material INSULATION, having constant material properties, was used and given the properties described in Table 1.

The time step chosen was 1 second (final time / 1800).

In Figure 5 is shown the distribution of the temperatures in the cross-section determined by SAFIR for the time $t = 1800$ s.

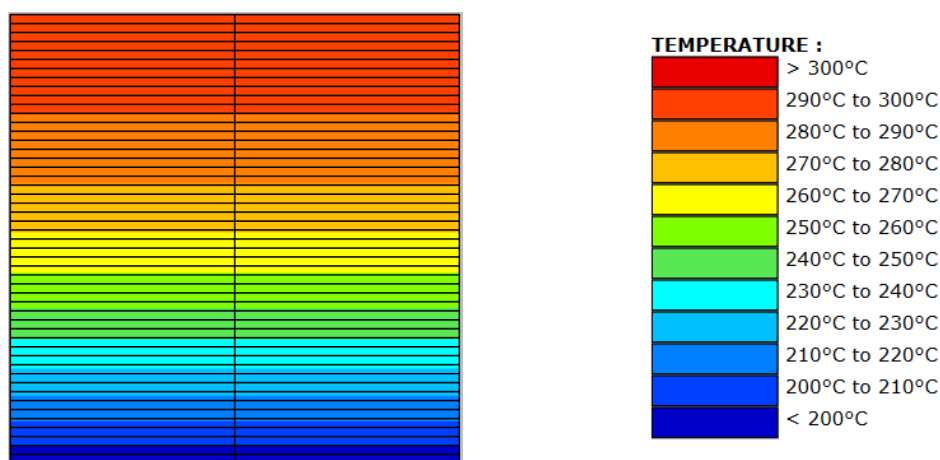


Figure 5 – Temperatures determined by SAFIR for Example 1, for $t = 1800$ s

Table 2 shows the temperatures obtained by SAFIR and those given as reference by the DIN.

Table 2 – Temperatures θ_0 at point X for Example 1

Time t	Reference temperature θ_0	Calculated temperature θ'_0	Deviation	
			$(\theta'_0 - \theta_0)$	$(\theta'_0 - \theta_0) / \theta_0 \cdot 100$
s	°C	°C	K	%
0	1000	1000	0.00	0.00
60	999.3	999.20	-0.10	-0.01
300	891.8	891.80	0.00	0.00
600	717.7	717.78	0.08	0.01
900	574.9	574.99	0.09	0.02
1200	460.4	460.52	0.12	0.03
1500	368.7	368.84	0.14	0.04
1800	295.3	295.42	0.12	0.04
Limits			±5.00	±1.00

It can be seen that the deviations fall well within the intervals of values defined in the DIN.

2.1.5 Analysis of the influence of different parameters

In this sub-chapter, an analysis of the sensibility of the results to different parameters is done. This will provide some indications on the minimum value of the time step or minimum number of nodes necessary in order to accurately simulate the cooling down process on the cross-section, as well as to confirm that the solution converges to a value as the mesh is refined.

2.1.5.1. Influence of the time step (see folder DIN1_5_1)

The mesh shown in Figure 5 was used here, and values of the time step equal to 1s, 5s, 10s, 20s, 30s, and 60s were tested. In Figure 4 are displayed the temperature distributions for four of these time steps, for the final time of 30min.

Figure 7 shows the evolution of the differences between the results from SAFIR and the ones of Annex CC as a function of time, depending on the value of the time step considered in the analysis.

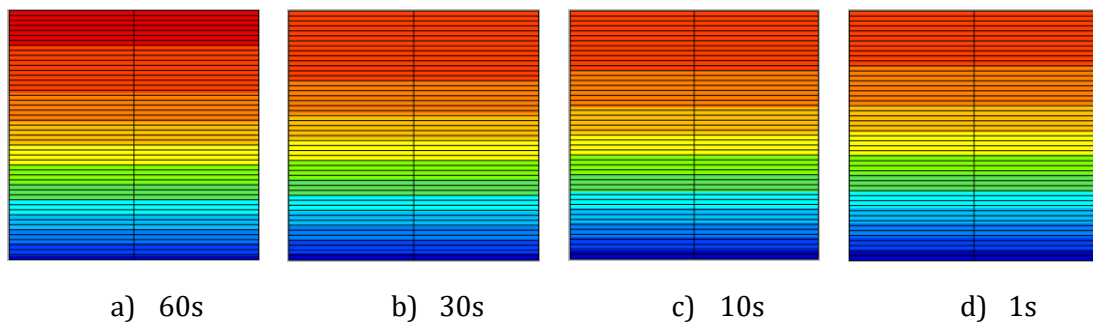


Figure 6 – Temperatures determined by SAFIR for some of the time steps tested, for $t = 1800s$ (colour scale is the same as in Figure 5)

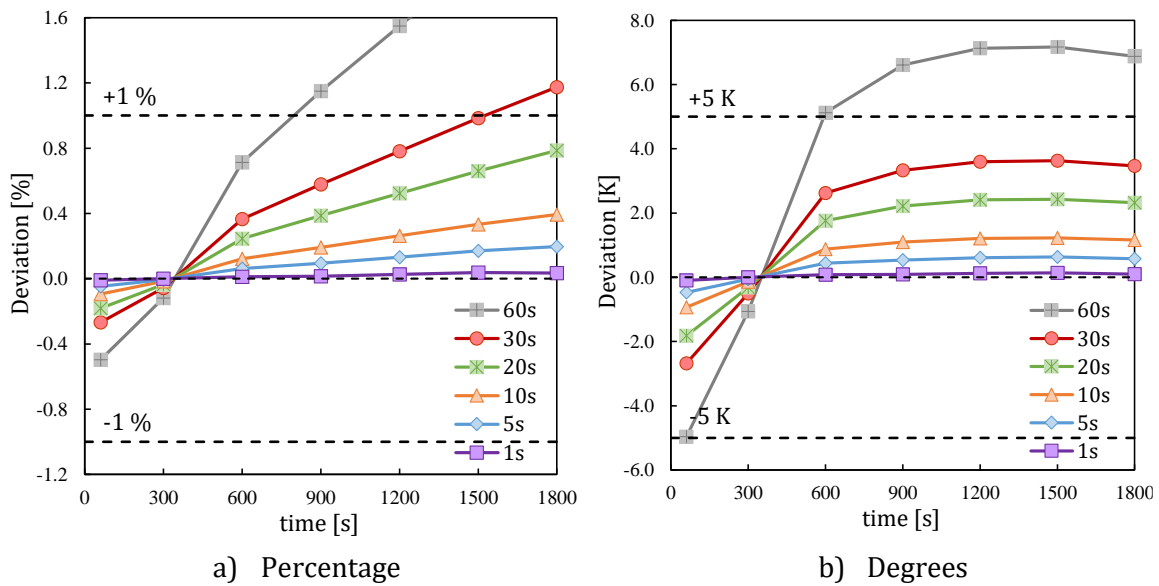


Figure 7 – Differences between the results by SAFIR and the reference results for different time steps

Different observations can be made on the last Figure:

- Apart from the first 300s, the deviation is systematically positive;
- After 600s, the deviation in terms of % increases linearly with time;
- The deviation in terms of K seems to remain more or less constant after 600s;
- Both criteria given in DIN are met as long as the time step does not exceed 25 s (final time/72). If only the absolute difference in K is considered, a time step of 40 s (final time/45) is acceptable.

2.1.5.2. Influence of the number of nodes (see folder DIN1_5_2)

To assess the influence of the refinement of the mesh on the results, different meshes, with still two elements on the horizontal direction but a varying number of elements on the direction of the heat flow, are analysed here considering analyses with a time step = 1s.

In Figure 8 are shown some of the meshes that were used. The temperatures determined after 30 min are plotted in Figure 9 for the meshes in Figure 8. The results for the deviations from the DIN found for all the meshes tested are presented in Figure 10.

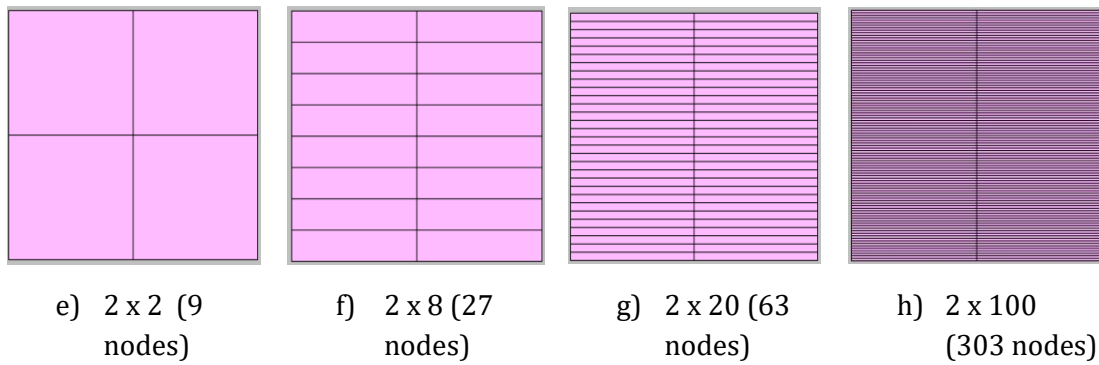


Figure 8 – Some of the meshes used in the study regarding the influence of the number of nodes on the results

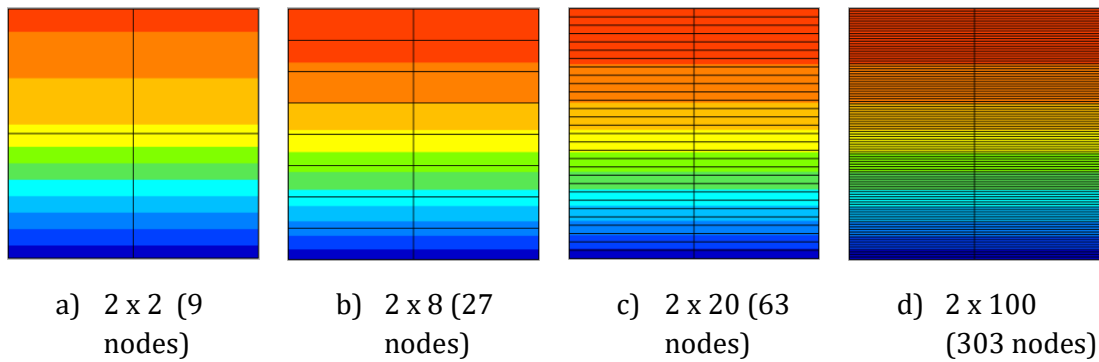


Figure 9 – Temperatures determined by SAFIR for some of the meshes used to study the influence of the number of nodes, for $t = 1800s$ (colour scale is the same as in Figure 5)

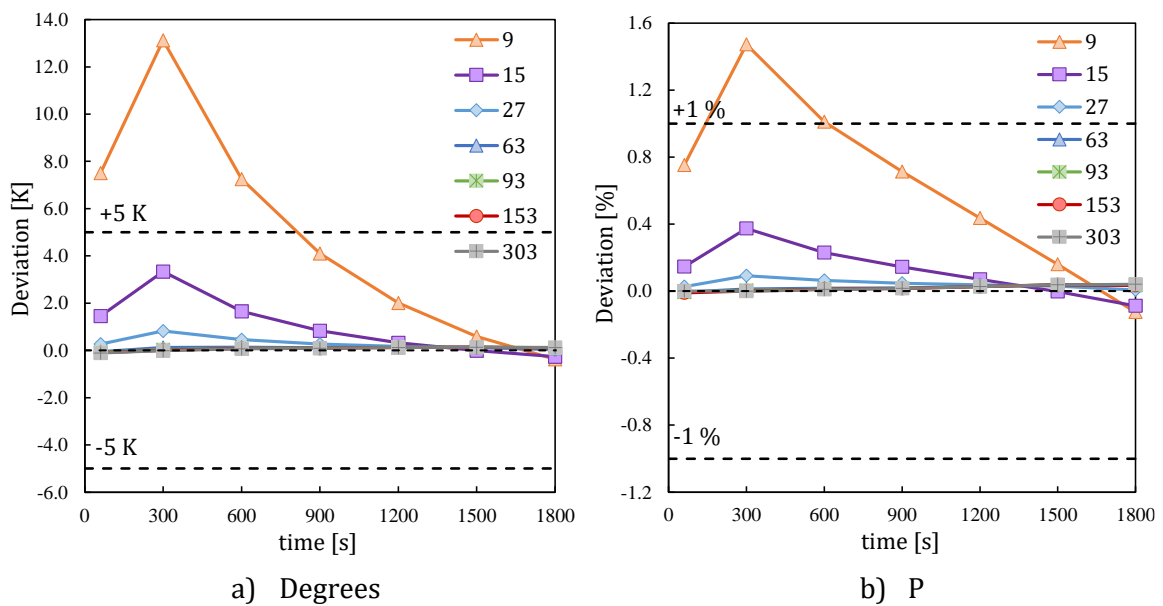


Figure 10 – Deviations of the results by SAFIR from the reference results for quadrilateral meshes with different densities (expressed in number of nodes)

Figure 10 shows that the models have converged when having more than 27 nodes (i.e. 7 nodes on the depth of the model), and that the results are within the limits defined in the DIN for meshes with as few as 4 nodes on the depth (or 15 nodes in total), if a grid configuration with two elements on the width is respected.

2.1.5.3. *Influence of the element type (see folder DIN1_5_3)*

A study was done in order to understand how the utilisation of triangles can affect the results. With that purpose, the crudest mesh from Figure 8 was taken as reference and triangle meshes with identical number and distribution of nodes were tested. Again, the time step here considered was for all cases equal to 1s.

The results for the temperatures at the top edge nodes of the cross-section are shown in Figure 11 and Figure 12 for $t = 1800s$, for the quadrilateral mesh and the meshes with triangles, respectively.

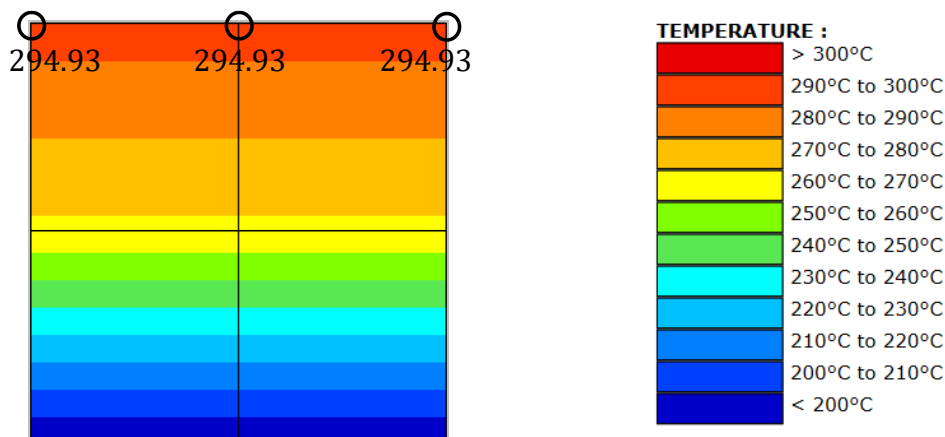


Figure 11 – Temperatures determined by SAFIR at the top 3 nodes for a quadrilateral mesh with 2x2 elements (9 nodes), for $t = 1800s$

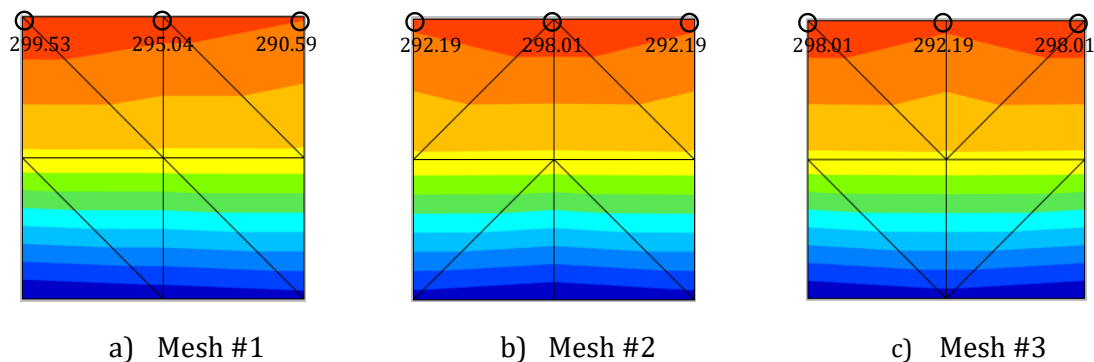


Figure 12 – Temperatures determined by SAFIR at the top 3 nodes for three different triangle meshes with 9 nodes each for $t = 1800s$ (colour scale is the same as in Figure 5)

It can be seen that for the three triangle meshes in Figure 12 the results depend on the arrangement of the triangles within the mesh, and that for the same mesh the nodes at the top edge show different values, unlike what happens with the quadrilateral mesh in Figure 11.

With a doubly symmetric mesh like the one in Figure 13, the same temperatures are obtained for the nodes with the same vertical position, as it is shown by the values plotted in that Figure for the top edge.

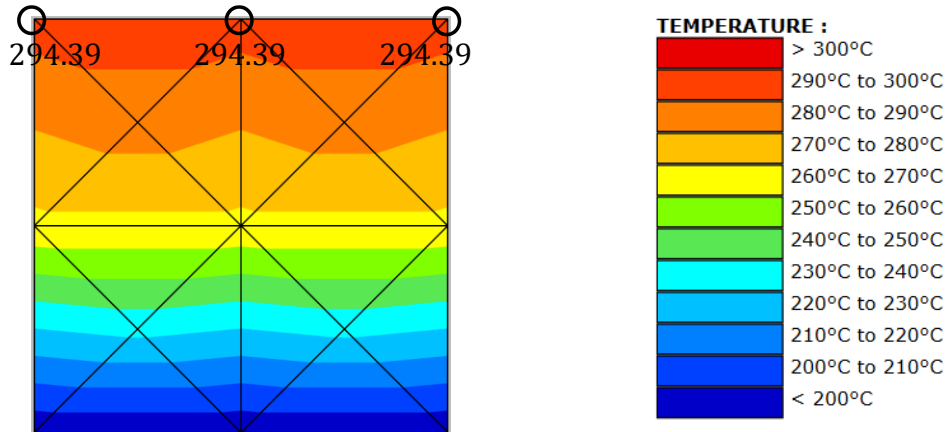


Figure 13 – Temperatures determined by SAFIR at the top 3 nodes for a doubly-symmetric triangle mesh with 13 nodes, for $t = 1800s$

Based on the latter, double symmetrical triangle meshes will be further compared to similarly refined models based on quadrilateral elements. For example, the triangle mesh in Figure 13 will be compared to the one presented in Figure 14.

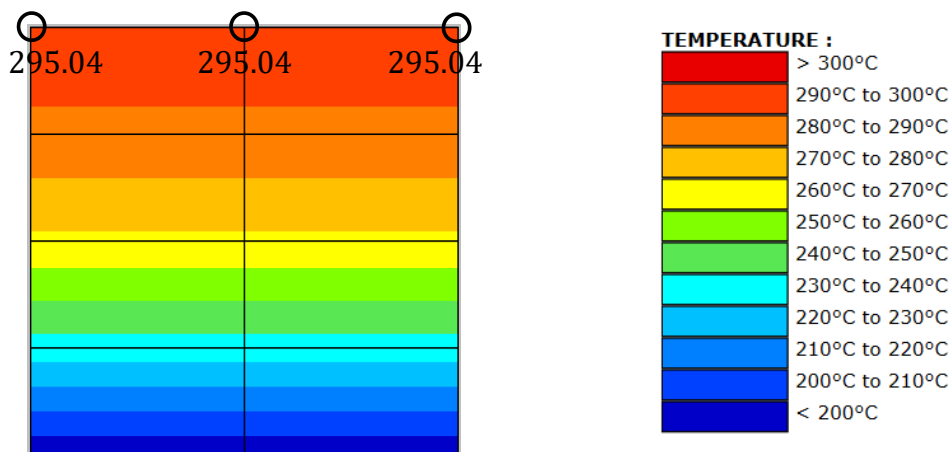


Figure 14 – Temperatures determined by SAFIR at the top 3 nodes for a quadrilateral mesh with 15 nodes, for $t = 1800s$

Figure 15 and Figure 16 show all the meshes tested. The distribution of the temperatures in the cross-sections are plotted in Figure 17 for $t = 1800s$, and the results for the temperature at the studied point are plotted in Figure 18.

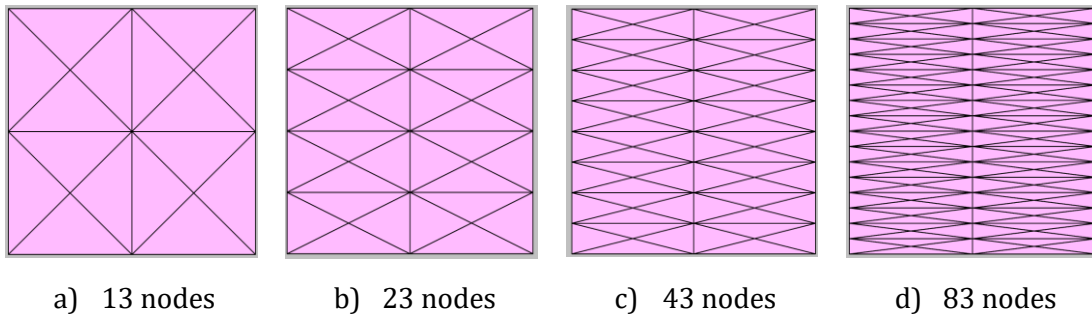


Figure 15 – Triangle meshes used to study the influence of the type of element on the results

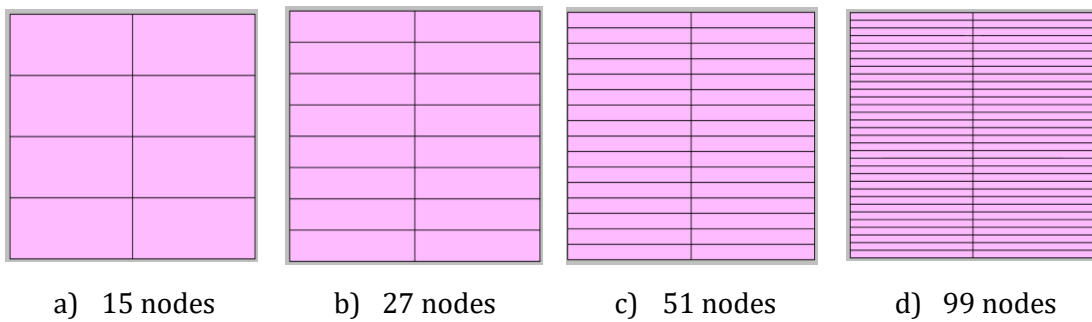


Figure 16 – Quadrilateral meshes used to study the influence of the type of element on the results

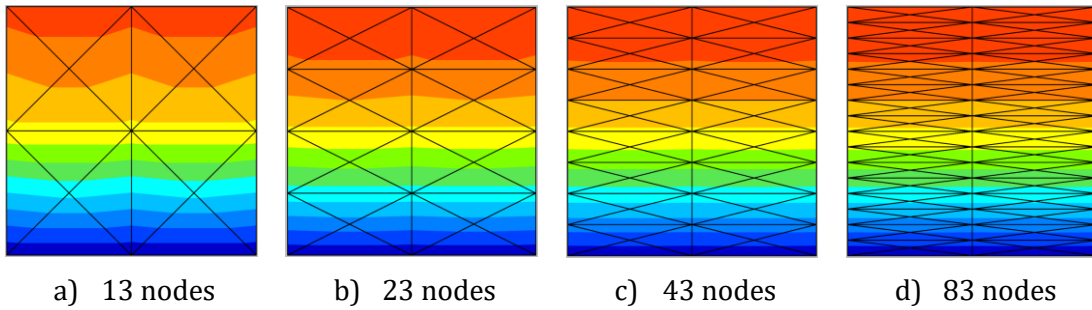


Figure 17 – Temperatures determined by SAFIR for triangle meshes, for $t = 1800s$ (colour scale is the same as in Figure 5)

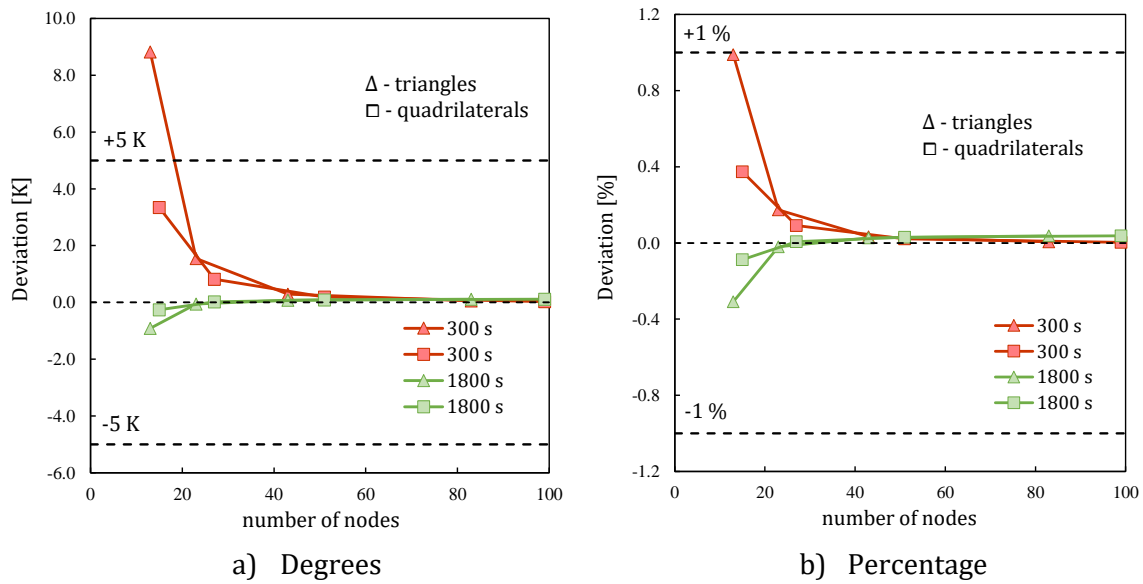


Figure 18 – Deviations of the results by SAFIR from the reference results for meshes with triangles and quadrilateral elements (expressed in number of nodes)

By observing the plots in Figure 18 one can see that, for the two crudest meshes related to each element type, the ones with quadrilaterals return the more accurate results and seem to converge faster to the solution implemented in SAFIR. However, this should be at least partially justified by the difference on the number of nodes between the models with quadrilaterals and triangles. As for the other meshes tested, it seems that for meshes with more than 23 nodes a convergence on the results is attained, regardless of the element type.

As for finding the crudest mesh able to return valid results according to the DIN, based on the plots above a mesh formed with triangles with slightly more than 13 nodes seems to be sufficiently refined for that purpose.

2.1.5.4. Influence of distorted meshes (see folder DIN1_5_4)

In order to understand what is the impact of the distortion of elements in the mesh, the 4 meshes present in Figure 19 and their undistorted counterparts in Figure 20 were analysed, considering a time step = 1s. The distribution of the temperatures in the cross-section is plotted in Figure 21 for $t = 1800s$, and the deviations of the results from the DIN with both types of meshes can be found in Figure 22.

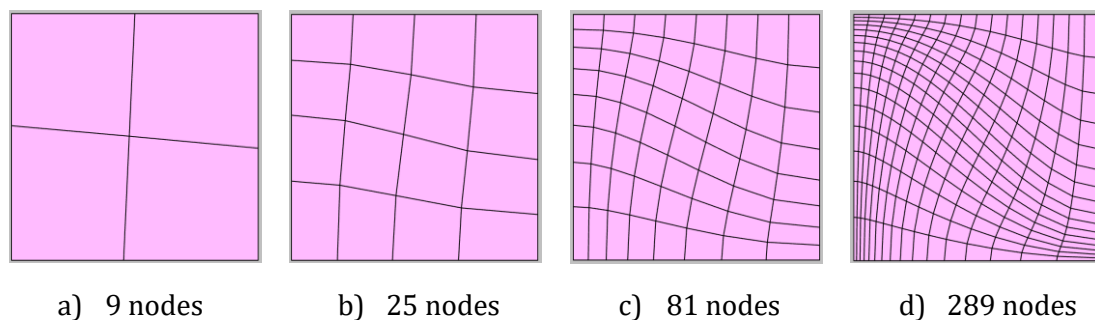


Figure 19 – Distorted meshes used to study the influence of distortion of elements on the results

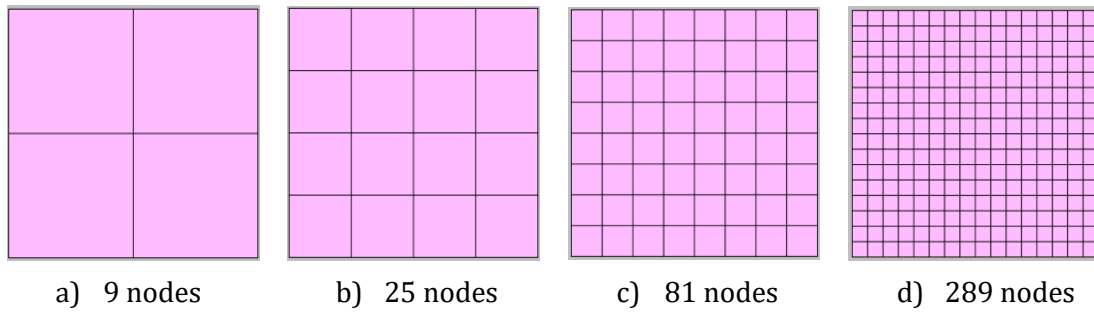


Figure 20 – Undistorted meshes used to study the influence of distortion of elements on the results

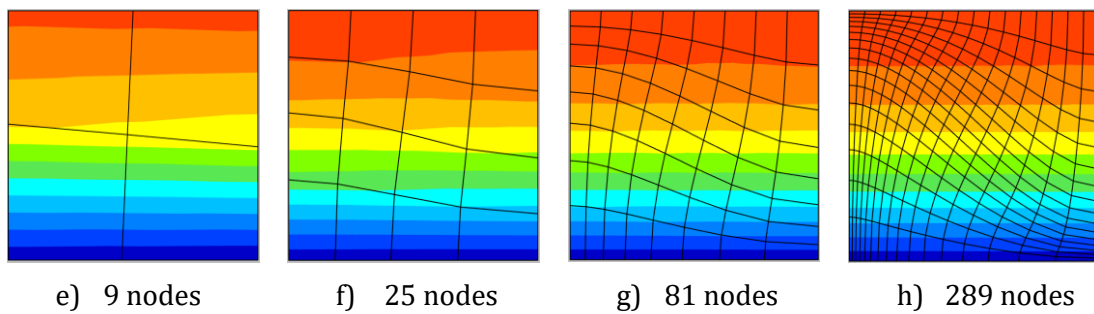


Figure 21 – Temperatures determined by SAFIR for the distorted meshes, for $t = 1800s$ (colour scale is the same as in Figure 5)

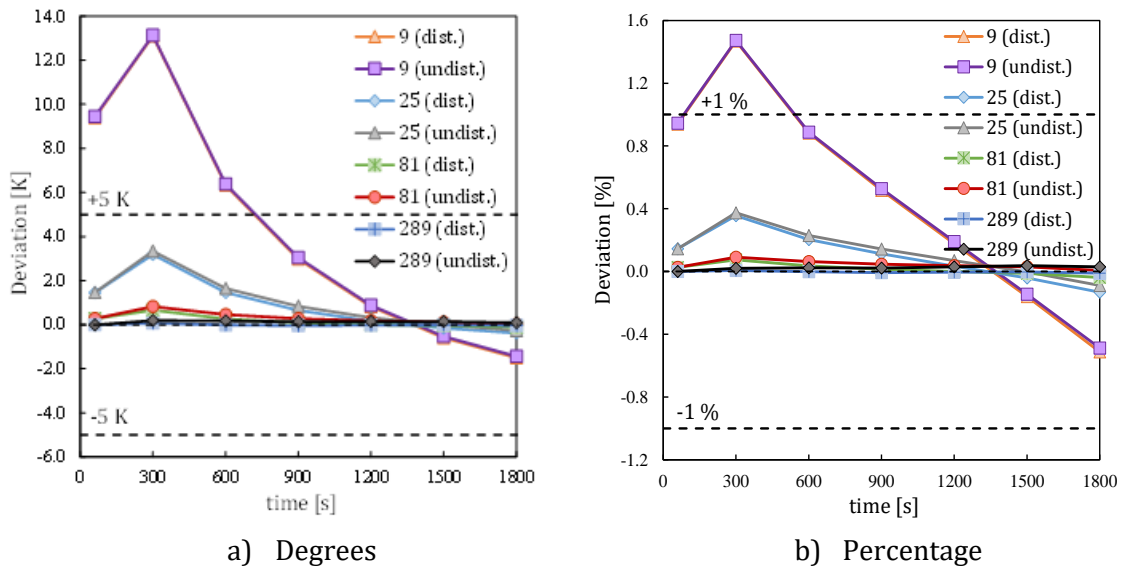


Figure 22 – Deviations of the results by SAFIR from the reference results for the distorted and undistorted meshes (expressed in number of nodes)

By looking at Figure 22 it is seen that by using distorted meshes the results deviate only slightly from the ones obtained with equivalent undistorted meshes.

2.1.5.5. *Influence of unstructured meshes (see folder DIN1_5_5)*

As a last step of this parametric analysis, the influence of using unstructured meshes is investigated. The 6 unstructured meshes present in Figure 23 are analysed, again considering a time step = 1s. The distribution of the temperatures in the cross-section is plotted in Figure 24 for $t = 1800s$, and the deviations of the results from the DIN can be found in Figure 25.

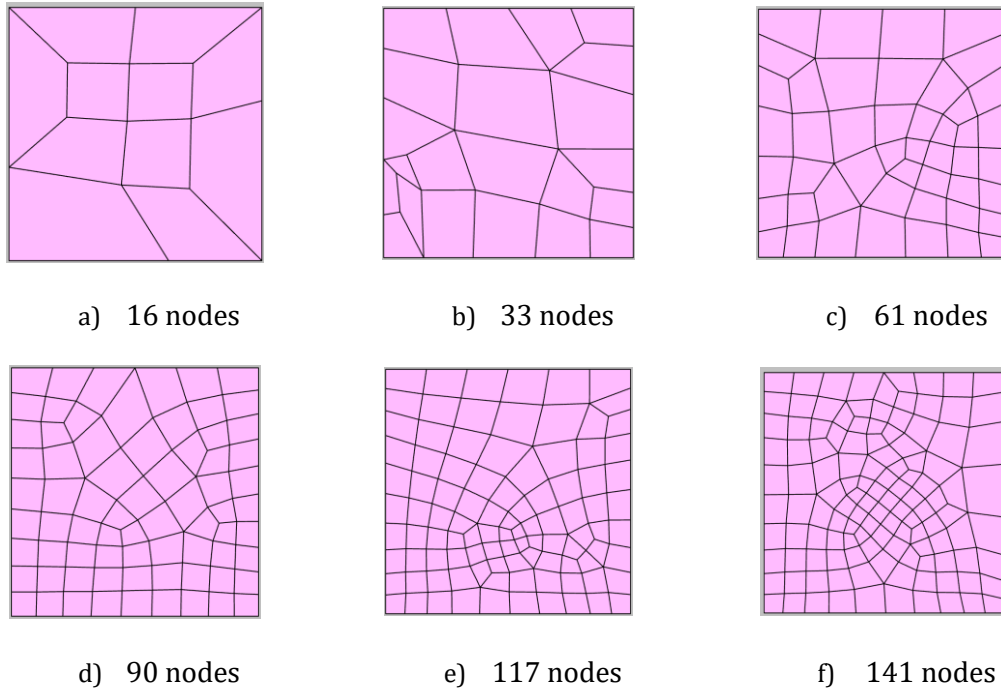


Figure 23 – Meshes used to study the influence of unstructured meshes on the results

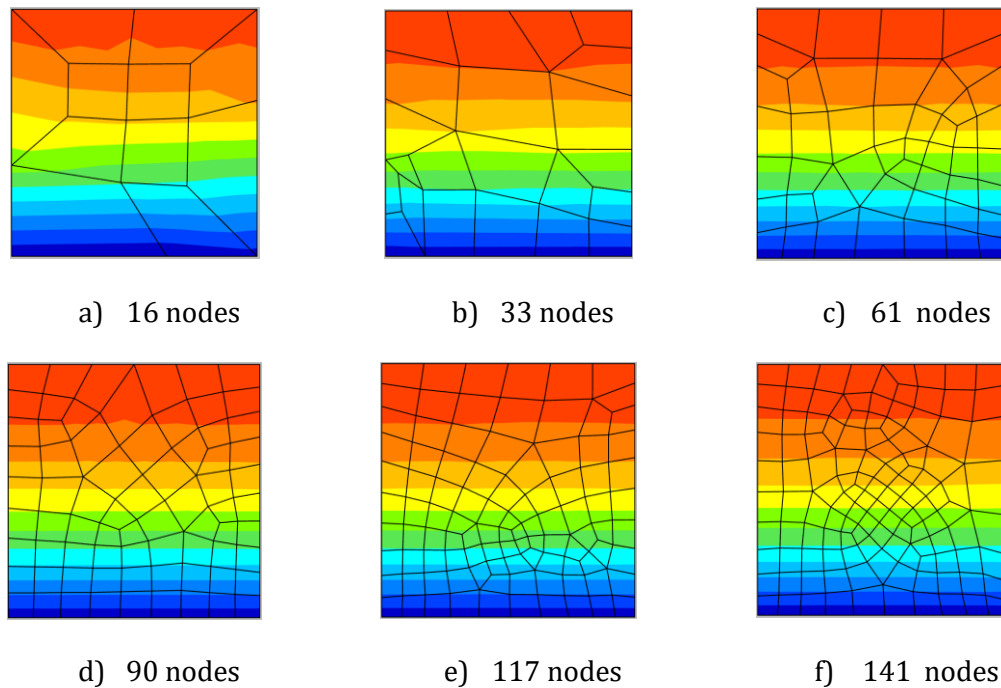


Figure 24 – Temperatures determined by SAFIR for the unstructured meshes, for $t = 1800s$ (colour scale is the same as in Figure 5)

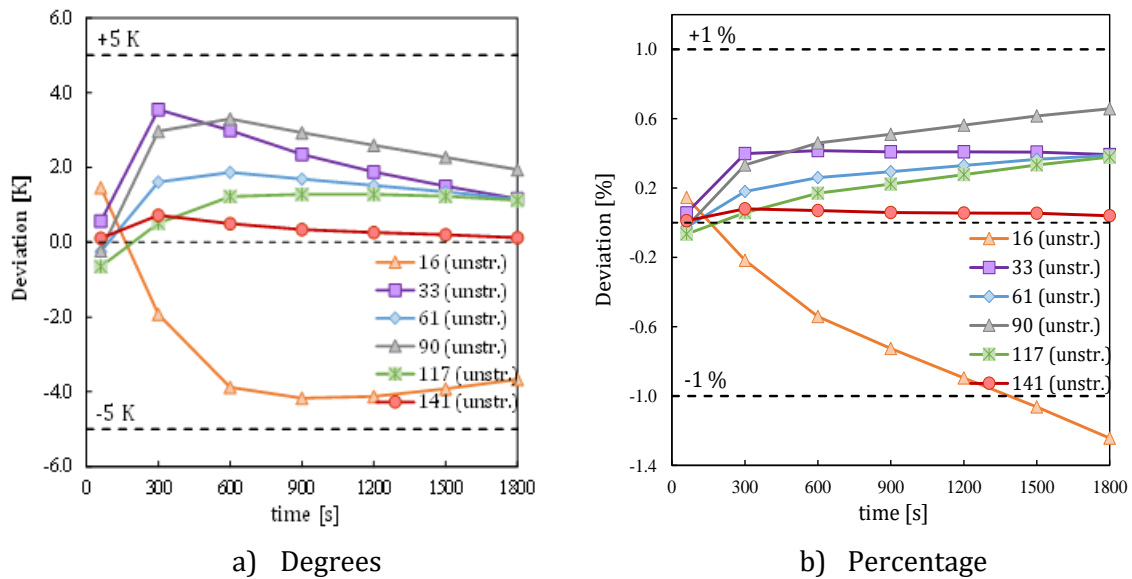


Figure 25 – Deviations of the results by SAFIR from the reference results for the unstructured meshes (expressed in number of nodes)

One can observe from Figure 25 that:

- Overall, the results with unstructured meshes are well placed inside the stipulated values;
- Crude unstructured meshes like the one with 16 nodes therein present can lead to some deviations from the reference results (although relatively small);
- Unstructured meshes are less efficient and often require more nodes to attain the same level of results than structured ones, as it is proved by the fact that the unstructured mesh with 113 nodes in Figure 25 still presents some considerable deviations, whereas in Figure 22 a mesh with just 81 nodes was able to attain very close results to the ones found in the DIN;
- A very good agreement between the results from SAFIR and the DIN was achieved when using an unstructured mesh with 141 nodes.

2.1.6 Conclusions

The parametric analysis shows that the solution of SAFIR satisfies the requirement of the standard. The solution converges to the theoretical solution when the density of the mesh is increased and the value of the time step is reduced.

When refining the mesh, rectangular elements converge slightly faster than triangular element; regular structured meshes are most efficient, with slight differences being observed in distorted structured meshes; unstructured meshes are somehow less efficient while being still in the acceptable range of the standard.

2.2. Example 2 – Heat transfer (heating) with varying properties

2.2.1 Keywords

Heat-transfer, conduction, convection, radiation, varying thermal properties

2.2.2 Objective

The goal of this example is to analyse the heat transfer by conduction when the thermal conductivity varies with the temperature, as well as the heat exchange with a gas at the boundary of the section by convection.

2.2.3 Description of the problem

A square section with the characteristics defined in Figure 26 and Table 3 is analysed. The temperature in the cross-section is uniform and equal to 0°C at time $t = 0$, when it is exposed to a gas with a temperature of 1000°C on all the edges. Heat transfer from the gas to the solid is by linear convection and radiation. In order to validate the results, the temperature θ_0 calculated at the centre of the cross-section is compared to the reference values presented in DIN EN1992-1-2 NA at different times, for a total duration of 3 hours.

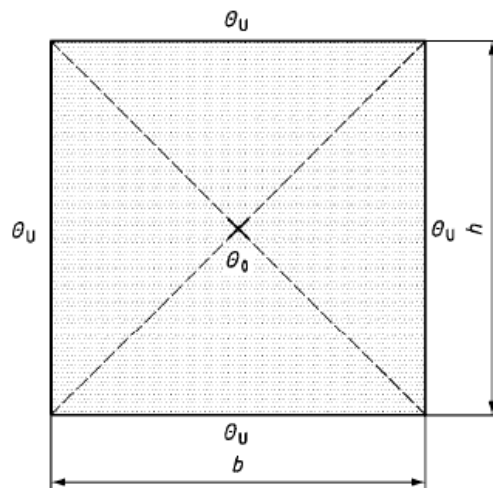


Figure 26 – Example 2: Heating up process in section with varying properties

Table 3 – Dimensions, material properties and boundary conditions for Example 2

Properties		Value	
Thermal conductivity λ (linear behaviour)	W / (m·K)	θ	$\lambda (\theta)$
		0	1.5
		200	0.7
		1000	0.5
Specific heat c_p	J / (kg·K)	1000	
Density ρ	Kg / m ³	2400	
Dimensions h, b	mm	200	
Coefficient of convection α_c	W / (m ² ·K)	10	
Emissivity $\epsilon_{res} = \epsilon_m \cdot \epsilon_f$	-	0.8	
Ambient temperature θ_u	°C	1000	
Initial temperature in the cross-section θ_{cs}	°C	0	

The data of this exercise are similar to that of a 20x20 cm² concrete section.

2.2.4 Model and results (see folder DIN2 4)

A model with a structured mesh formed by 576 square elements (24 by 24) was created. Each of these elements contains 2 gauss points of integration in its plane, and the total number of nodes is 625.

The initial temperature in the structure was set to 0°C, and a FRONTIER constraint of 1000°C was applied to all faces of the cross-section by the function “F1000”, as seen in Figure 27.

The PRECISION command was set to 1.0E-3. A USER material was applied according to the properties described in Table 3. The time step chosen was 10 seconds (final time / 1080).

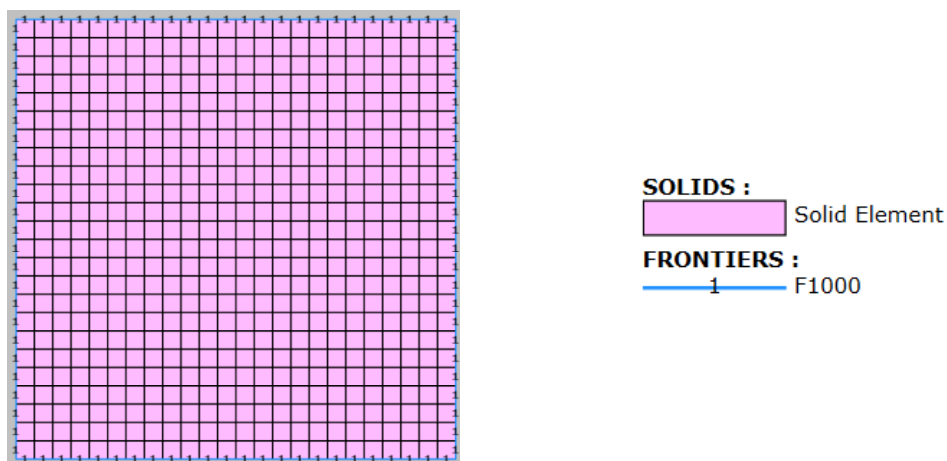


Figure 27 – Thermal model of the cross-section for Example 2 (24 x 24 SOLID elements)

Figure 28 shows the temperature distribution for the final target time of 180 min.

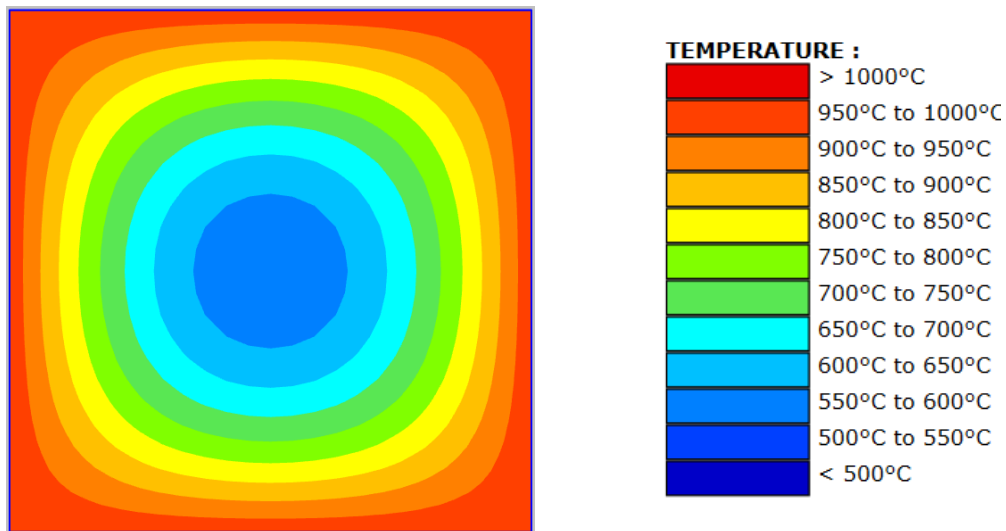


Figure 28 – Temperatures determined by SAFIR for Example 2, for $t = 180\text{min}$

Table 4 gives the temperatures obtained by SAFIR and those given as reference by the DIN. All the differences are within the boundaries stipulated by the DIN.

Table 4 – Temperatures θ_0 for Example 2

Time	Reference temperature	Calculated temperature	Deviation	
t	θ_0	θ'_0	$(\theta'_0 - \theta_0)$	$(\theta'_0 - \theta_0) / \theta_0 \cdot 100$
min	°C	°C	K	%
30	36.9	32.18	-4.72	-12.79
60	137.4	132.40	-5.00	-3.64
Limit ($t \leq 60\text{min}$)			± 5.00	
90	244.6	241.67	-2.93	-1.20
120	361.1	362.75	1.65	0.46
150	466.2	469.83	3.63	0.78
180	554.8	559.93	5.13	0.92
Limit ($t > 60\text{min}$)				± 3.00

2.2.5 Analysis of the influence of different parameters

In this sub-chapter, an analysis of the sensibility of the results to different input parameters is done. This will provide some indications on the minimum value of the time step or minimum number of nodes necessary in order to accurately simulate the heating process on the cross-section, as well as to confirm that the solution converges to a value as the mesh is refined.

2.2.5.1. Influence of the time step (see folder DIN2_5_1)

To study the influence of the time step on the results, the mesh shown in Figure 27 was used, and values of the time step equal to 1, 5, 10, 20, 30, 60, 120, 300, 600 and 1200 s were tested.

Figure 29 shows the evolution of the differences between the results from SAFIR and the ones of Annex CC as a function of time, depending on the value of the time step considered in the analysis. The areas of the chart with a white background represent the domain where the criteria, either in terms of percentage or in degrees, must be applied.

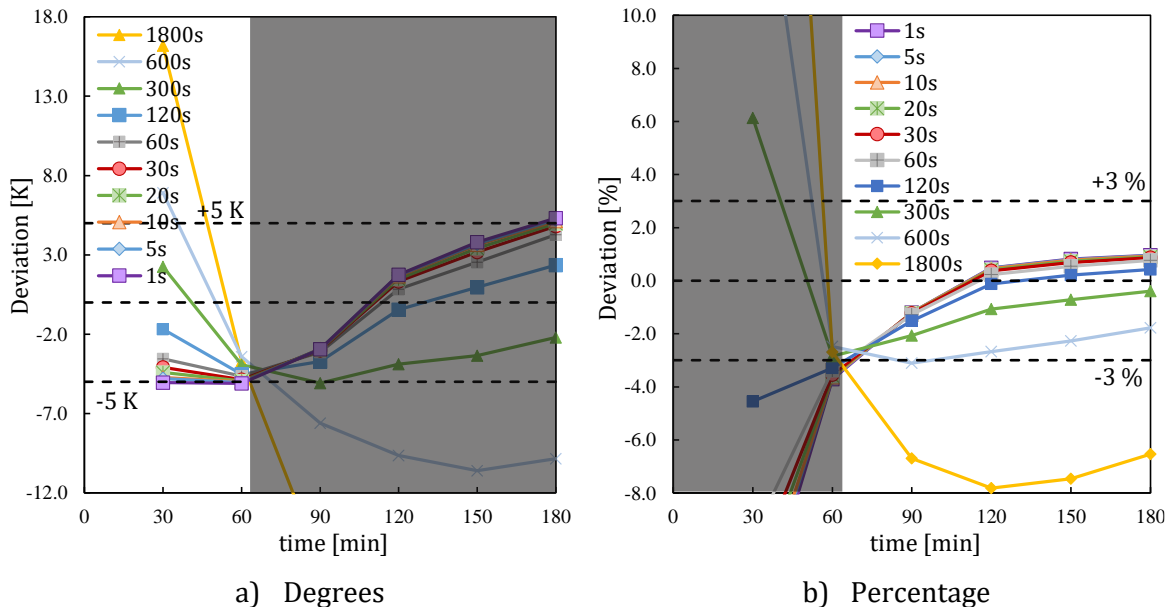


Figure 29 – Differences between the results by SAFIR and the reference results for different time steps

Different observations can be made on the last Figure:

- For the values of the time steps between 1s and 300s, inclusive, all the results fall within the intervals, considering the zones of application of each criteria (percentage or Kelvin degrees);
- When considering the absolute difference in Kelvin, considerable differences between the different time steps are obtained for $t = 30$ min, where bigger time steps consistently return bigger temperatures. For this time instant, the time step that returns a temperature value identical to the reference seems to be somewhere between 120s and 300s. For $t = 60$ min these differences practically disappear.
- For the range of application of the limit in percentage, the results provided are valid for time steps of less than 600s, inclusive, with bigger time steps consistently returning lower temperatures, contrary to what happens for the first 60 min.

2.2.5.2. *Influence of the number of nodes (see folder DIN2_5_2)*

To assess the influence of the refinement of the mesh on the results, 6 different meshes are analysed considering analyses with a time step = 10s. All meshes were defined as a grid with equal number of elements in each direction, respectively 2x2, 4x4, 8x8, 16x16, 24x24 and 50x50.

Figure 30 shows part of the meshes that are used. The temperatures determined after 180 min are plotted in Figure 31 for those meshes. The results for the deviations from the DIN found for all the meshes tested are presented in Figure 32.

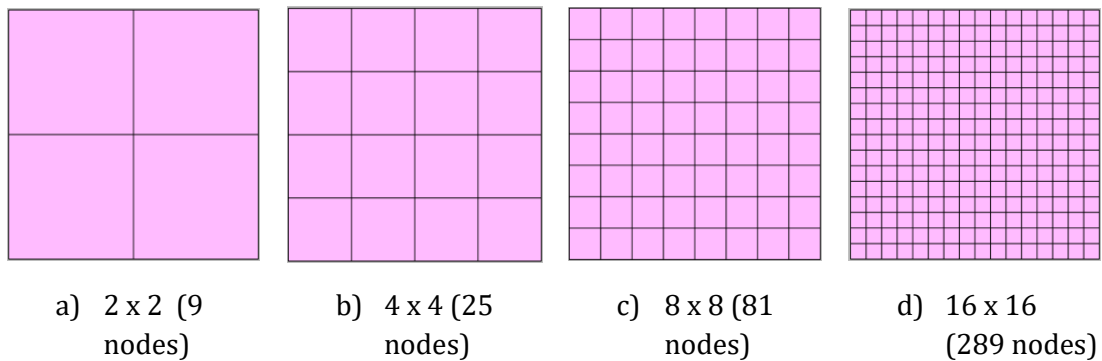


Figure 30 – Meshes used to study the influence of unstructured meshes on the results

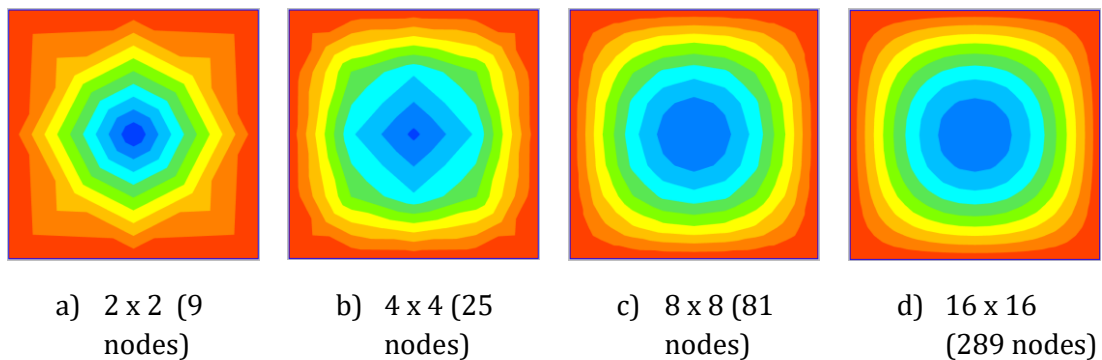


Figure 31 – Temperatures determined by SAFIR for some of the meshes used to study the influence of the number of nodes, for $t = 180\text{min}$ (colour scale is the same as in Figure 28)

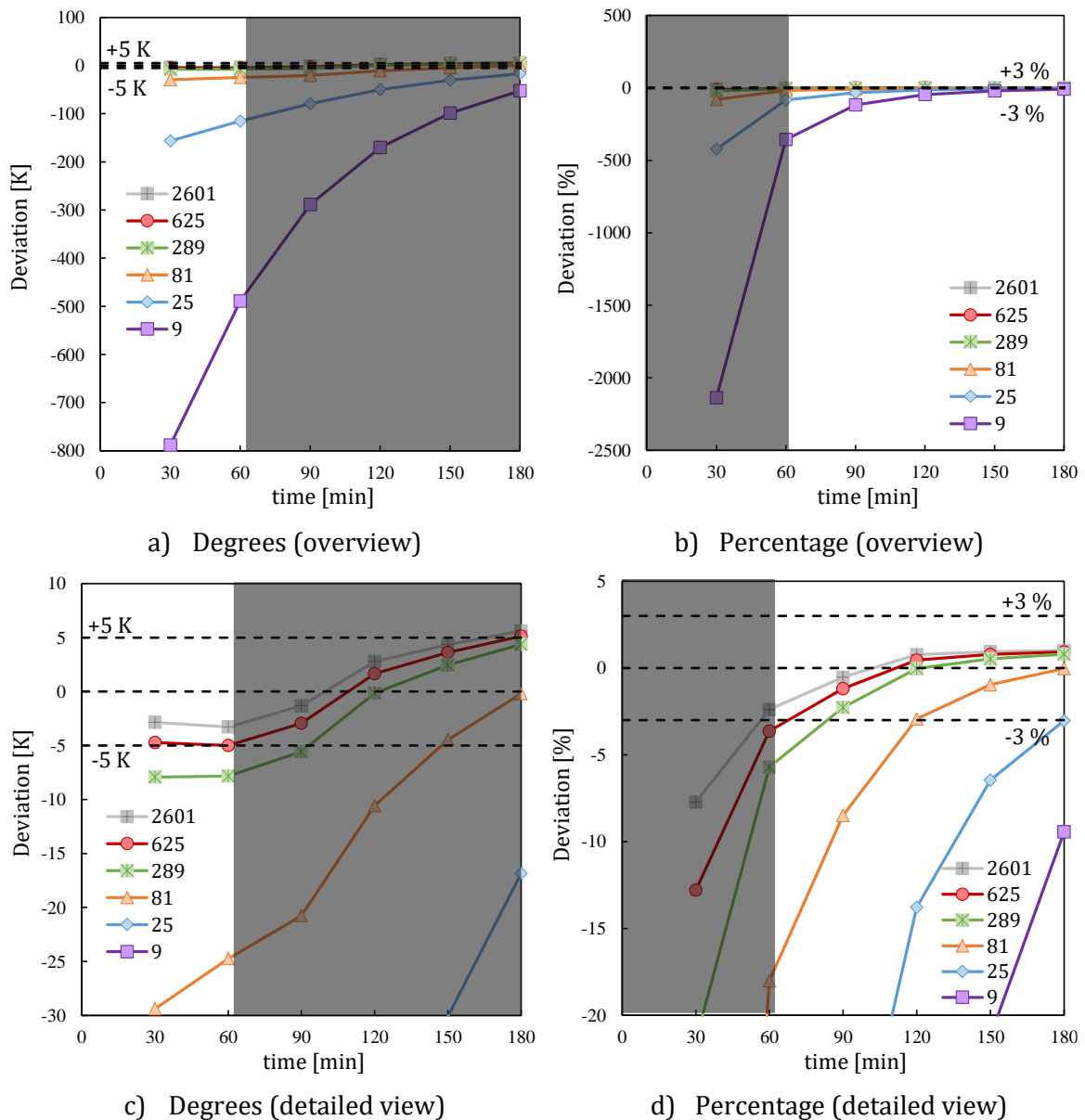


Figure 32 – Differences between the results by SAFIR and the reference results for quadrilateral meshes with different densities (expressed in number of nodes)

The following comments can be made on Figure 32:

- The crudest meshes analysed returned results that are hugely and negatively affected by the skin effect – the use of a reduced number of consecutive linear functions as an approximation to a parabolic solution;
- Considering the stipulated boundaries, meshes with at least 625 nodes are able to provide valid results for the whole range of time steps analysed (this corresponds to element thickness of 8.3 mm);
- The mesh with 289 nodes (12.5 mm thick elements) is able to provide good results for the range covered by the limitation in terms of percentage, but not for the one in terms of degrees.

- It seems therefore as if 10 mm is approximately the limit for the thickness of element layers near the surface in concrete type sections.

2.2.5.3. Influence of the element type (see folder DIN2_5_3)

The influence of the type of element is analysed by means of 4 different triangle meshes compared with 4 quadrilateral meshes with a time step of 10 s.

Figure 33 and Figure 34 show the meshes tested. The distributions of the temperatures in the triangle meshes are plotted in Figure 35.

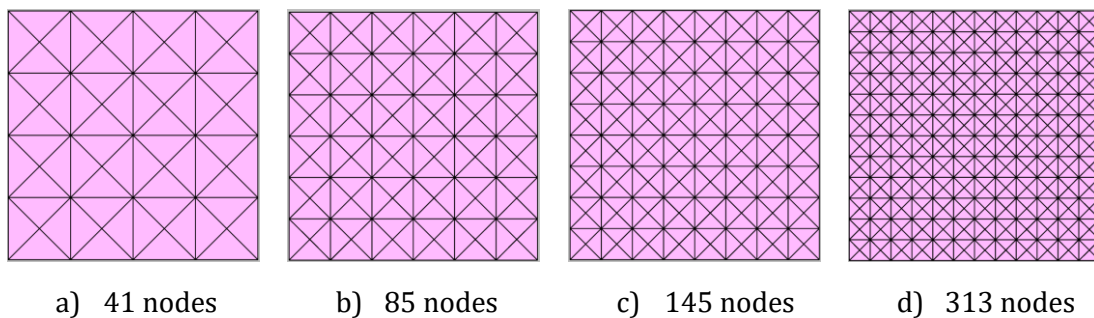


Figure 33 – Triangle meshes used to study the influence of the type of element on the results

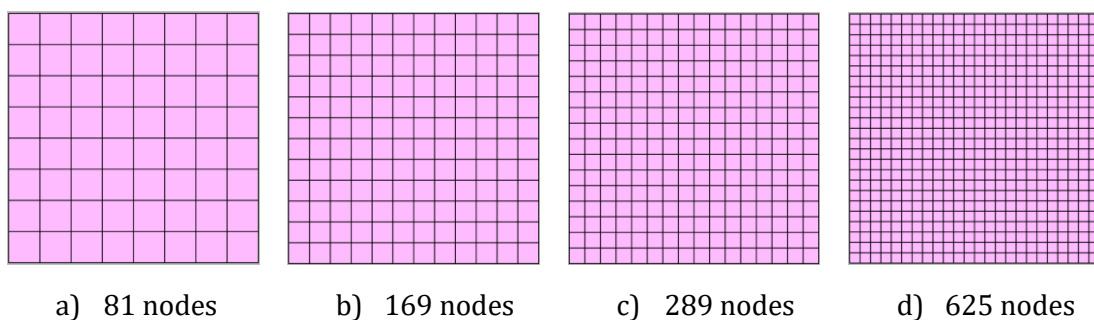


Figure 34 – Quadrilateral meshes used to study the influence of the type of element on the results

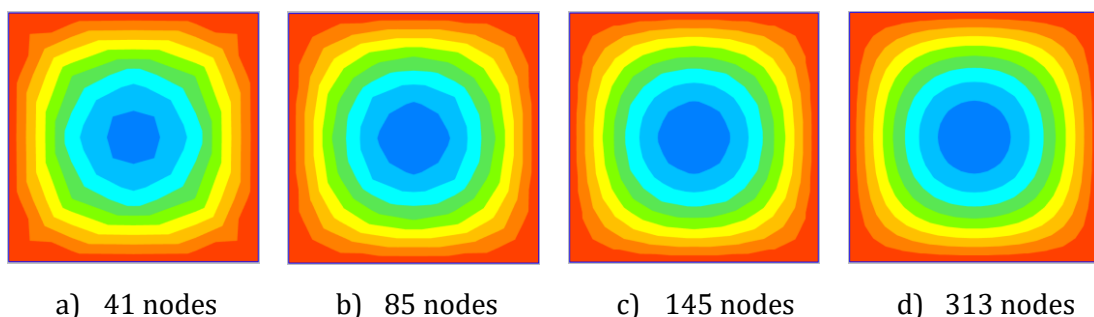


Figure 35 – Temperatures determined by SAFIR for the triangle meshes, for $t = 180$ min (colour scale is the same as in Figure 28)

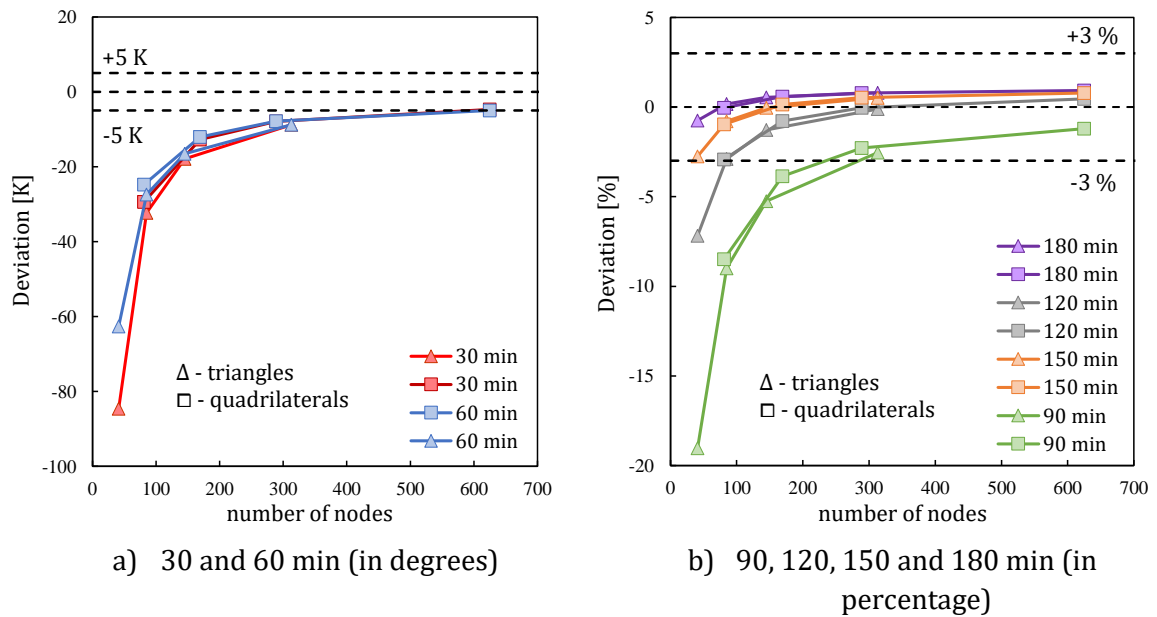


Figure 36 – Deviations of the results by SAFIR from the reference results for meshes with triangles and quadrilateral elements (expressed in number of nodes)

From Figure 40 it can be seen that the difference in the results between triangular elements and square elements are not significant (marginally better results are obtained with square elements).

2.2.5.4. Influence of unstructured meshes (see folder DIN2_5_4)

The influence of having unstructured meshes is investigated. The 4 meshes in Figure 37 were analysed, again considering a time step = 10s.

The distribution of the temperatures in the cross-section is plotted in Figure 38 for t = 180 min, and the deviations of the results from the DIN with the studied unstructured meshes are found in Figure 39.

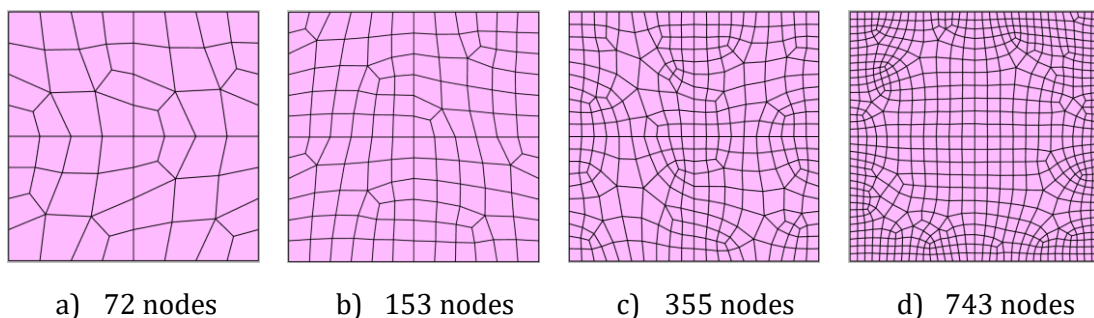


Figure 37 – Meshes used to study the influence of unstructured meshes on the results

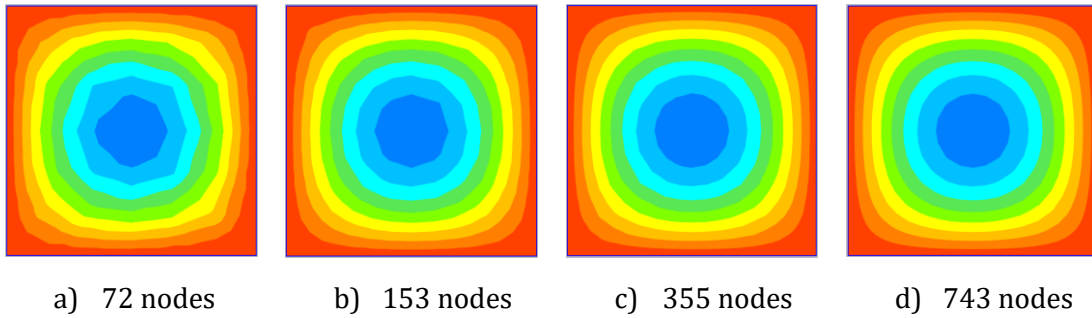


Figure 38 – Temperatures determined by SAFIR for the unstructured meshes, for $t = 180$ min (colour scale is the same as in Figure 28)

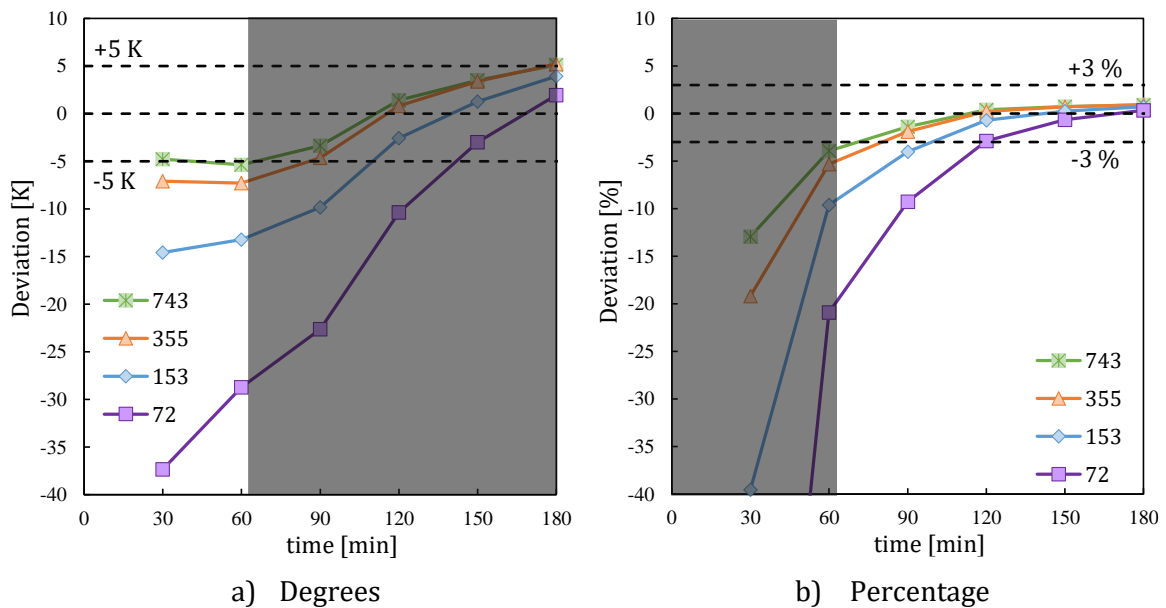


Figure 39 – Differences between the results by SAFIR and the reference results, for quadrilateral meshes with different densities (expressed in number of nodes)

The analysis of the results in Figure 39 allows to conclude that having an unstructured mesh doesn't greatly affect the results obtained, as a mesh with 743 nodes presents very identical results to the ones obtained with a structured mesh with 625 nodes (see Figure 33), which fall inside the DIN limits for all the range of time instants studied.

2.2.6 Conclusions

Like in Example 1, the parametric analysis has shown that the solution satisfies the requirement of the standard, provided that the mesh used is sufficiently refined.

It was noticed that meshes with quadrilateral elements converged slightly but not significantly faster than triangular elements, while no significant differences appeared between unstructured and structured meshes.

2.3. Example 3 – Heat transfer through several layers

2.3.1 Keywords

Heat-transfer, conduction, convection, radiation, various material layers

2.3.2 Objective

The goal of this example is to analyse the heat transfer in a steel hollow section that is filled with a lightweight insulating material. The thermal conductive properties of steel are those of EN 1993-1-2 whereas the filling material has constant thermal properties.

2.3.3 Description of the problem

A square section with the characteristics defined in Figure 40 and Table 5 is analysed. The temperature in the cross-section is uniform and equal to 0°C at time $t = 0$, when it is exposed to a gas with a temperature of 1000°C on all the edges. Heat transfer from the gas to the solid is by linear convection and by radiation. In order to validate the results, the temperature θ_0 calculated at the centre of the cross-section is compared to the reference values presented in DIN EN1992-1-2 NA, for a duration of 3 hours.

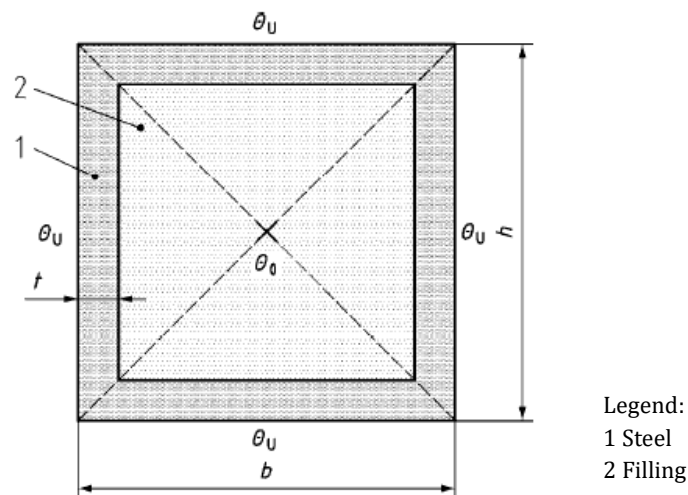


Figure 40 – Example 3: Heat-transfer through several layers

Table 5 – Dimensions, material properties and boundary conditions for Example 3

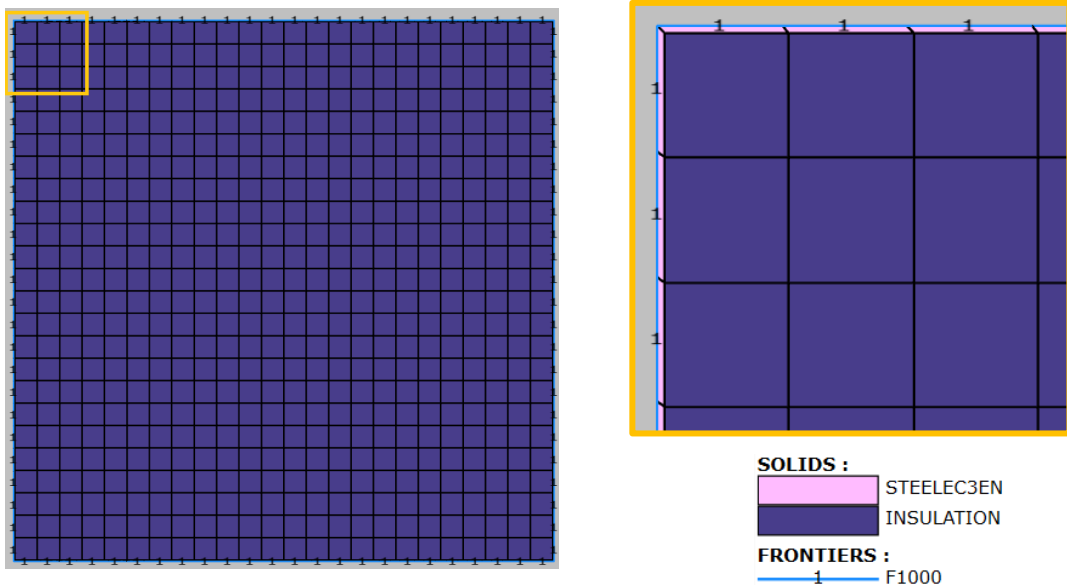
Properties		Steel	Filling
Thermal conductivity λ	W / (m·K)	EN 1993-1-2	0.05
Specific heat c_p	J / (kg·K)	EN 1993-1-2	1000
Density ρ	Kg / m ³	EN 1993-1-2	50
Dimensions h, b, t	mm	$h = b = 201, t = 0.5$	
Coefficient of convection α_c	W / (m ² ·K)	10	
Emissivity $\epsilon_{res} = \epsilon_m \cdot \epsilon_f$	-	0.8	
Initial temperature in the cross-section θ_{cs}	°C	0	0
Ambient temperature θ_u	°C	1000	

2.3.4 Model and results (see folder DIN3 4)

A model with a structured mesh formed by 672 quadrilateral elements was created, which consists on a grid of 24 x 24 elements for the filling material, with the steel hollow section being defined with also 24 elements along each edge of the section and 1 element across the thickness. Each of these elements contains 2 Gauss points of integration, and the total number of nodes is 721.

The initial temperature in the structure was set to 0°C, and a frontier constraint of 1000°C was applied to all the faces of the cross-section according to Figure 41.

The PRECISION command was set to 1.0E-3. An INSULATION material with constant material properties according to Table 5 was used for the filling, and the STEELEC3EN material was used for the hollow section, by changing the heat transfer coefficients at the surface to match the values in Table 5. The time step chosen was 10 s (final time / 1080).



a) Overall view

b) Detail of the two layers

Figure 41 – Thermal model of the cross-section for Example 3 (24 x 24 SOLID elements)

Figure 42 shows the temperature distribution for the final time of 180min.

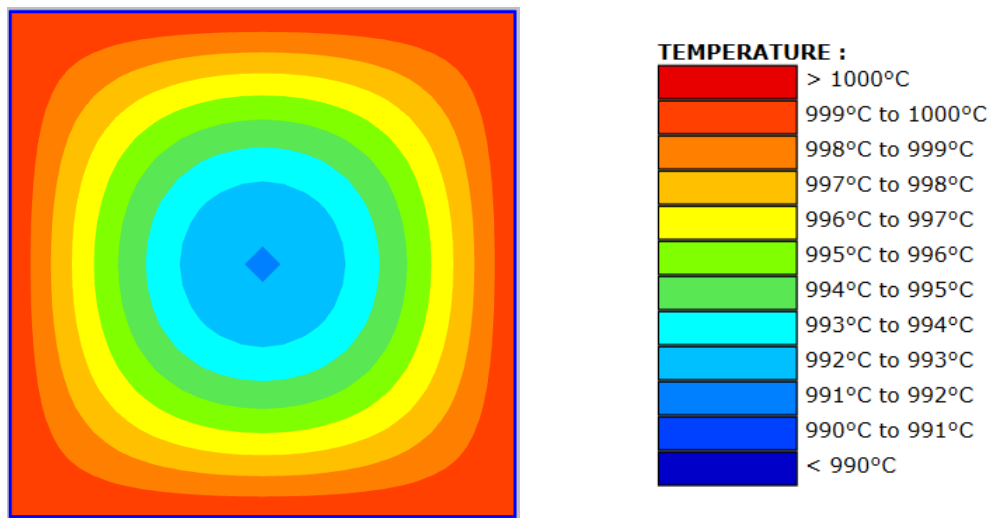


Figure 42 – Temperatures determined by SAFIR for Example 3, for $t = 180\text{min}$.

Table 6 shows the deviations of the temperatures obtained by SAFIR when compared to those given as reference by the DIN.

Table 6 – Temperature θ_0 for Example 3

Time	Reference temperature	Calculated temperature	Deviation	
			$(\theta'_0 - \theta_0)$	$(\theta'_0 - \theta_0) / \theta_0 \cdot 100$
t	θ_0	θ'_0	$(\theta'_0 - \theta_0)$	$(\theta'_0 - \theta_0) / \theta_0 \cdot 100$
min	°C	°C	K	%
30	340.5	338.89	-1.61	-0.47
60	717.1	721.97	4.87	0.68
90	881.6	885.24	3.64	0.41
120	950.6	952.66	2.06	0.22
150	979.3	980.47	1.17	0.12
180	991.7	991.95	0.25	0.03
Limits			±5.00	±1.00

2.3.5 Conclusions

The deviations found were within the limits stipulated by the DIN, both in absolute and in relative values, for the whole duration of the simulation.

2.4. Example 4 – Thermal expansion

2.4.1 Keywords

Thermal expansion, steel, homogenous temperature

2.4.2 Objective

The goal of this example is to analyse the thermal expansion of a steel member for different values of homogeneous temperature in a cross-section.

2.4.3 Description of the problem

A squared section with the characteristics defined in Figure 43 and Table 7 is analysed. In order to validate the results, the thermal elongation Δl at the simply supported end of the member is determined and compared to the reference values presented in DIN EN1992-1-2 NA.

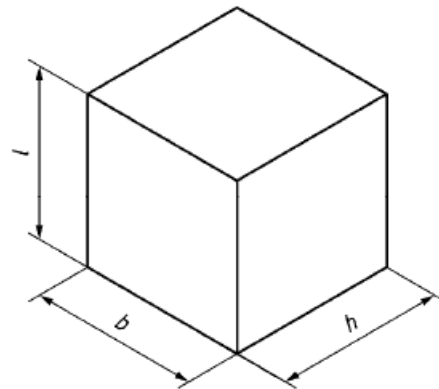


Figure 43 – Example 4: Thermal expansion in statically assembled member

Table 7 – Dimensions, material properties and boundary conditions for Example 4

Properties		Steel
Dimensions l, h, b	mm	100
Stress-strain material law		EN 1993-1-2
Yield strength f_{yk}	N /mm ²	355
Initial conditions	°C	20
Homogeneous temperature in the member θ_u	°C	100, 300, 500, 600, 700, 900
Thermal expansion		EN 1993-1-2

2.4.4 Model and results (see folder DIN4_4)

In this example the calculations were performed using BEAM 2D, BEAM 3D, TRUSS, SHELL and SOLID 3D elements, in order to get those different formulations validated.

No thermal analysis is presented here. The prescribed temperatures have been directly introduced in the relevant files for the structural analysis to be performed.

2D BEAM element

A 2D mechanical model with 1 BEAM element that is free to expand was created and exposed, unloaded, to the prescribed temperature fields.

In Figure 44 a representation of the thermal elongation determined by SAFIR is shown (in the Figure the elongation is causing the right support to move horizontally).



Figure 44 – Thermal elongation determined by SAFIR for Example4, for $t = 900^{\circ}\text{C}$, using a 2D BEAM element

Table 8 shows the deviations of the temperatures obtained by SAFIR when compared to those given as reference by the DIN.

Table 8 – Thermal elongation Δl for Example 4, using a 2D BEAM element

Temperature	Reference extension	Calculated extension	Deviation	
			$(\Delta l' - \Delta l)$	$(\Delta l' - \Delta l) / \Delta l \cdot 100$
θ	Δl	$\Delta l'$	mm	%
$^{\circ}\text{C}$	mm	mm	mm	%
100	0.09984	0.0998	-0.00004	-0.04
300	0.37184	0.372	0.00016	0.04
Limit ($\theta \leq 300^{\circ}\text{C}$)			± 0.05	
500	0.67584	0.676	0.00016	0.02
600	0.83984	0.84	0.00016	0.02
700	1.01184	1.01	-0.00184	-0.18
900	1.18000	1.18	0.00000	0.00
Limit ($\theta > 300^{\circ}\text{C}$)				± 1.00

3D BEAM element

A 3D mechanical model with 1 BEAM element that is free to expand was created and exposed, unloaded, to the prescribed temperature fields.

In Figure 45 a representation of the thermal elongation determined by SAFIR is shown (in the Figure the elongation is causing the support on the left to move according to the X-axis).

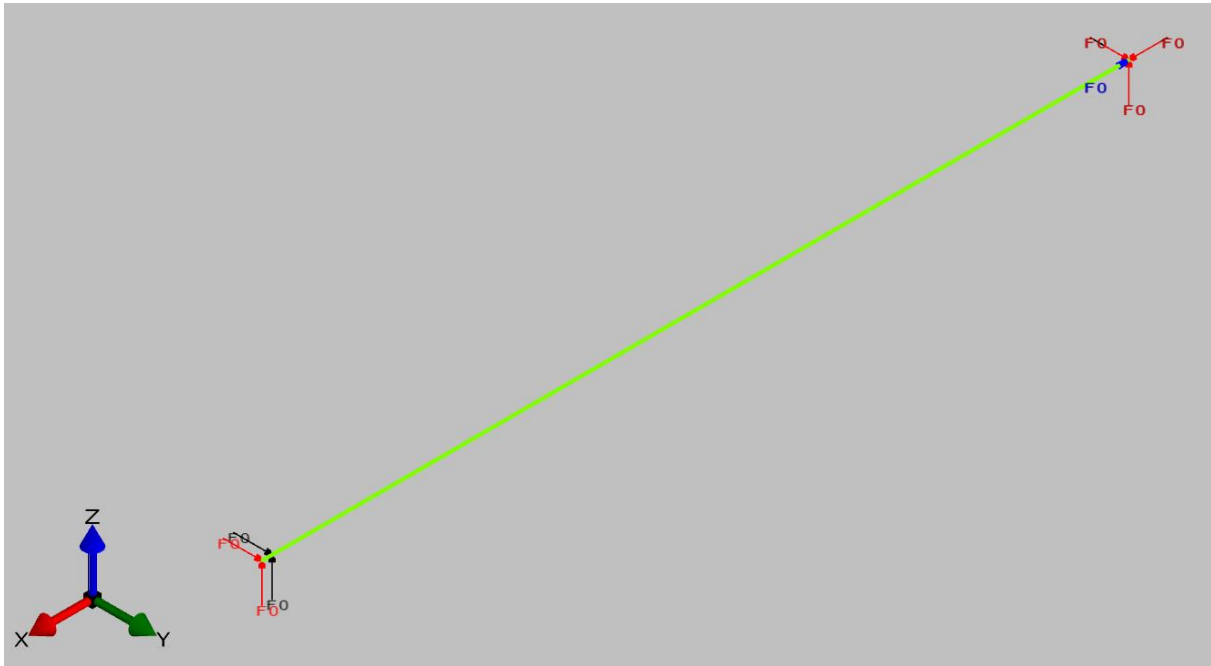


Figure 45 – Thermal elongation determined by SAFIR for Example 4, for $t = 900^{\circ}\text{C}$, using a 3D BEAM element

Table 10 shows the deviations of the temperatures obtained by SAFIR when compared to those given as reference by the DIN.

Table 9 – Thermal elongation Δl for Example 4, using a 3D BEAM element

Temperature	Reference extension	Calculated extension	Deviation	
			$(\Delta l' - \Delta l)$	$(\Delta l' - \Delta l) / \Delta l \cdot 100$
θ	Δl	$\Delta l'$	mm	%
$^{\circ}\text{C}$	mm	mm	mm	%
100	0.09984	0.0998	-0.00004	-0.04
300	0.37184	0.372	0.00016	0.04
Limit ($\theta \leq 300^{\circ}\text{C}$)			± 0.05	
500	0.67584	0.676	0.00016	0.02
600	0.83984	0.84	0.00016	0.02
700	1.01184	1.01	-0.00184	-0.18
900	1.18000	1.18	0.00000	0.00
Limit ($\theta > 300^{\circ}\text{C}$)				± 1.00

TRUSS element

A 2D mechanical model with 1 TRUSS element that is free to expand was created and exposed, unloaded, to the prescribed temperature fields.

In Figure 46 a representation of the thermal elongation determined by SAFIR is shown (in the Figure the elongation is causing the right support to move horizontally).



Figure 46 – Thermal elongation determined by SAFIR for Example 4, for $t = 900^{\circ}\text{C}$, using a TRUSS element

Table 10 shows the deviations of the temperatures obtained by SAFIR when compared to those given as reference by the DIN.

Table 10 – Thermal elongation Δl for Example 4, using a BEAM element

Temperature	Reference extension	Calculated extension	Deviation	
			$(\Delta l' - \Delta l)$	$(\Delta l' - \Delta l) / \Delta l \cdot 100$
θ	Δl	$\Delta l'$		
$^{\circ}\text{C}$	mm	mm	mm	%
100	0.09984	0.0998	-0.00004	-0.04
300	0.37184	0.371	-0.00084	-0.23
Limit ($\theta \leq 300^{\circ}\text{C}$)			± 0.05	
500	0.67584	0.674	-0.000184	-0.27
600	0.83984	0.836	-0.000384	-0.46
700	1.01184	1.01	-0.00184	-0.18
900	1.18000	1.17	-0.01000	-0.85
Limit ($\theta > 300^{\circ}\text{C}$)				± 1.00

SHELL element

A 3D mechanical model with 9 SHELL elements (3x3) that is free to expand was created and exposed, unloaded, to the prescribed temperature fields.

The visualization in DIAMOND of the displacements obtained by SAFIR in one of the directions is shown in Figure 47 (the same results were obtained for the expansion in both directions).

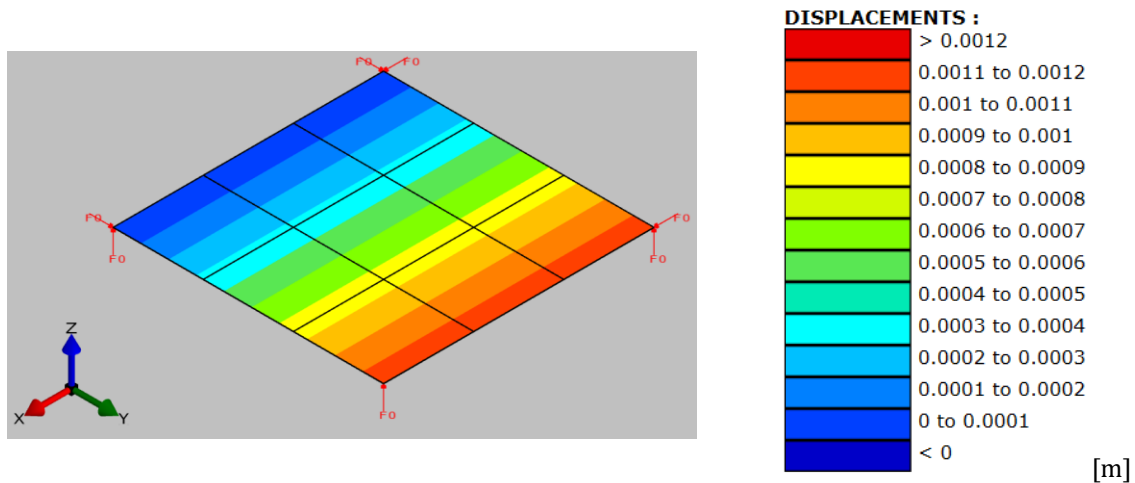


Figure 47 – Thermal elongation in Y-direction determined by SAFIR for Example 4, for $t = 900^{\circ}\text{C}$, using SHELL elements

Table 11 shows the deviations of the temperatures obtained by SAFIR when compared to those given as reference by the DIN.

Table 11 – Thermal elongation Δl for Example 4, using SHELL elements

Temperature	Reference extension	Calculated extension	Deviation	
			$(\Delta l' - \Delta l)$	$(\Delta l' - \Delta l) / \Delta l \cdot 100$
θ	Δl	$\Delta l'$	Mm	%
$^{\circ}\text{C}$	mm	mm		
100	0.09984	0.0998	-0.00004	-0.04
300	0.37184	0.371	-0.00084	-0.23
Limit ($\theta \leq 300^{\circ}\text{C}$)			± 0.05	
500	0.67584	0.674	-0.000184	-0.27
600	0.83984	0.836	-0.000384	-0.46
700	1.01184	1.01	-0.00184	-0.18
900	1.18000	1.17	-0.01000	-0.85
Limit ($\theta > 300^{\circ}\text{C}$)				± 1.00

SOLID elements

A 3D mechanical model with 1 SOLID element that is free to expand was created and exposed, unloaded, to the prescribed temperature fields.

The visualization in DIAMOND of the displacements obtained by SAFIR in one of the directions is shown in Figure 48 (the same results were obtained for the expansion in all 3 directions).

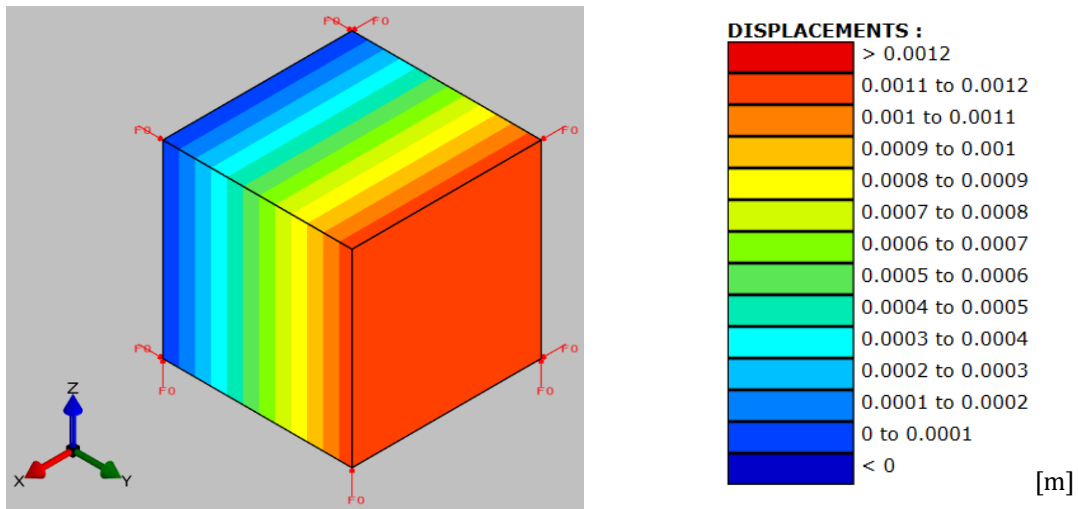


Figure 48 – Thermal elongation in Y-direction determined by SAFIR for Example 4, for $t = 900^{\circ}\text{C}$, using a SOLID element

Table 12 shows the deviations of the temperatures obtained by SAFIR when compared to those given as reference by the DIN.

Table 12 – Thermal elongation Δl for Example 4, using a SOLID element

Temperature	Reference expansion	Calculated expansion	Deviation	
			$(\Delta l' - \Delta l)$	$(\Delta l' - \Delta l) / \Delta l \cdot 100$
θ	Δl	$\Delta l'$	mm	%
$^{\circ}\text{C}$	mm	mm	mm	%
100	0.00984	0.0998	-0.00004	-0.04
300	0.37184	0.372	0.00016	0.04
Limit ($\theta \leq 300^{\circ}\text{C}$)			± 0.05	
500	0.67584	0.676	0.00016	0.02
600	0.83984	0.84	0.00016	0.02
700	1.01184	1.01	-0.00184	-0.18
900	1.18000	1.18	0.00000	0.00
Limit ($\theta > 300^{\circ}\text{C}$)				± 1.00

2.4.5 Conclusions

The results calculated for all types of elements are within the limits stipulated by the DIN.

It may appear inconsistent that, in one single software, the thermal expansion is not exactly the same for all types of elements. Indeed, for 900°C , for example, the 2D BEAM, the 3D BEAM and the SOLID finite elements yield an expansion of 1.18 mm, which is exactly the expected value, whereas the TRUSS and the SHELL finite elements yield a value of 1.17 mm.

The reason lies in the fact that the axial strain is calculated based on a linearized expression in the SOLID elements (because they are written in a small displacements formulation) and in the BEAM finite elements (because these are expected to deflect essentially in bending rather than in elongation).

$$\varepsilon = \frac{l - l_i}{l_i}$$

On the contrary, for the TRUSS elements where elongation is the sole deformation and in SHELL elements that can also work as membrane elements, the more correct nonlinear expression is being used.

$$\varepsilon = \frac{l^2 - l_i^2}{2 l_i^2}$$

It can be verified that, with an elongation of 1.17 mm from an initial length of 100 mm, the second expression yields a strain equal to 1.1768 %. If, by multiplying the length of the specimen by a factor of 10, one gains access to an additional significant digit, the elongation for the BEAM and the SOLID elements is found as 1.173 mm, which yields a strain of 1.1799 %.

The results are thus consistent with the fact that thermal strain of steel in SAFIR is calculated in the same manner for all element types, in full accordance with the recommendation of EN 1993-1-2.

2.5. Example 5 - Temperature-dependent stress-strain curves of concrete and steel

2.5.1 *Keywords*

Elongation, column, steel, concrete, homogenous temperature

2.5.2 *Objective*

The goal of this example is to analyse the total elongation of a column made of steel or concrete for different uniform temperature distributions at some given stress-strength ratios.

2.5.3 *Description of the problem*

Members with the characteristics defined in Figure 49 and Table 13 are analysed. In order to validate the results, the elongation Δl at the unsupported end of the members is determined and compared to the reference values presented in DIN EN1992-1-2 NA.

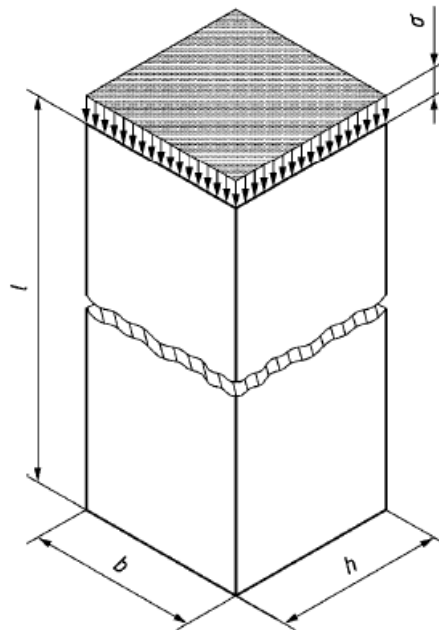


Figure 49 – Example 5: Temperature-dependent stress-strain in column (stability failure is excluded)

Table 13 – Dimensions, material properties and boundary conditions for Example 5 and Example 6

Properties		Steel	Concrete ^a
Dimensions l, h, b	mm	100, 10, 10	100, 31.6, 31.6
Stress-strain material law		EN 1993-1-2	EN 1992-1-2
Yield strength $f_y(20^\circ\text{C})$, $f_c(20^\circ\text{C})$	N/mm ²	355	20
Thermal expansion		EN 1993-1-2	EN 1992-1-2
Initial conditions	°C	20	
Homogeneous temperature in the member θ	°C	20, 200, 400, 600, 800	
Load $\sigma_s(\theta) / f_y(\theta)$ and $\sigma_c(\theta) / f_c(\theta)$		0.2, 0.6, 0.9	
^a – with predominantly siliceous aggregates			

2.5.4 Models and results (see folder DIN5 4)

A 2D mechanical model with 1 BEAM element was created and replicated in order to be associated to the 15 different combinations of the temperatures with the stress / strength ratios. Static analyses with a PRECISION of 10E-3s, a COMEBACK of 1s and a time step of 60s were performed for each case.

This was done for both steel and concrete using the materials STEELEC3EN and SILCONC_EN and the properties in Table 13. The results obtained are shown, respectively, in Table 14 and Table 15.

Table 14 – Elongation Δl for the steel column in Example 5

Temp.	Stress / Strength	Red. Coeff.	Applied force	Ref. value	Calc. value	Deviation	
θ	$\sigma_{S\theta} / f_{yk}(\theta)$	$k_{y,\theta} = f_{y,\theta}/f_y$	$F_{c\theta}$	Δl	$\Delta l'$	$(\Delta l' - \Delta l)$	$(\Delta l' - \Delta l) / \Delta l \cdot 100$
°C	-	-	N	mm	mm	mm	%
20	0.2	1	-7100	-0.034	-0.0338	0.0002	-0.59
	0.6	1	-21300	-0.101	-0.101	0.0000	0.00
	0.9	1	-31950	-0.152	-0.152	0.0000	0.00
200	0.2	1	-7100	0.194	0.194	0.0000	0.00
	0.6	1	-21300	0.119	0.119	0.0000	0.00
	0.9	1	-31950	-0.159	-0.159	0.0000	0.00
400	0.2	1	-7100	0.472	0.472	0.0000	0.00
	0.6	1	-21300	0.293	0.293	0.0000	0.00
	0.9	1	-31950	-0.451	-0.451	0.0000	0.00
600	0.2	0.47	-3337	0.789	0.789	0.0000	0.00
	0.6	0.47	-10011	0.581	0.581	0.0000	0.00
	0.9	0.47	-15017	-0.162	-0.162	0.0000	0.00
800	0.2	0.11	-781	1.059	1.06	0.0010	0.09
	0.6	0.11	-2343	0.914	0.915	0.0010	0.11
	0.9	0.11	-3515	0.170	0.171	0.0010	0.59
Limit							± 3.00

Table 15 – Elongation Δl for the concrete column in Example 5

Temp.	Stress / Strength	Red. Coeff.	Applied force	Ref. value	Calc. value	Deviation	
θ	$\frac{\sigma_{s\theta}}{f_{yk}(\theta)}$	$f_{c,\theta}/f_{ck}$	$F_{c\theta}$	Δl	$+\Delta l'$	$(\Delta l' - \Delta l)$	$\frac{(\Delta l' - \Delta l)}{\Delta l} \cdot 100$
$^{\circ}\text{C}$	-	-	N	mm	mm	mm	%
20	0.2	1	-3994	-0.0334	-0.0334	0.0000	0.00
	0.6	1	-11983	-0.104	-0.104	0.0000	0.00
	0.9	1	-17974	-0.176	-0.176	0.0000	0.00
200	0.2	0.95	-3795	0.107	0.107	0.0000	0.00
	0.6	0.95	-11384	-0.0474	-0.0474	0.0000	0.00
	0.9	0.95	-17075	-0.2075	-0.207	0.0005	-0.24
400	0.2	0.75	-2996	0.356	0.356	0.0000	0.00
	0.6	0.75	-8987	0.075	0.075	0.0000	0.00
	0.9	0.75	-13481	-0.216	-0.216	0.0000	0.00
600	0.2	0.45	-1797	0.685	0.685	0.0000	0.00
	0.6	0.45	-5392	-0.0167	-0.0167	0.0000	0.00
	0.9	0.45	-8088	-0.744	-0.744	0.0000	0.00
800	0.2	0.15	-599	1.066	1.07	0.0040	0.38
	0.6	0.15	-1797	0.365	0.365	0.0000	0.00
	0.9	0.15	-2696	-0.363	-0.363	0.0000	0.00
Limit							± 3.00

2.5.5 Conclusions

For both steel and concrete, the major part of the cases returned exactly the same value as the reference. Whenever this was not the case, the differences found were minor and well within the boundaries stipulated by the DIN, and those were related to the number of significant digits produced by SAFIR in .xml file and displayed in DIAMOND.

Calculations were also performed using the TRUSS and the BEAM 3D elements, for the cases with 600°C and a stress / strength ratio of 0.6, which returned the same (or virtually the same) results as for the BEAM 2D cases, for both steel and concrete.

2.6. Example 6 – Temperature-dependent limit-load-bearing capacity of concrete and steel

2.6.1 Keywords

Ultimate bearing capacity, column, steel, concrete, homogeneous temperature

2.6.2 Objective

The goal of this example is to determine the load bearing capacity at different homogeneous temperatures for the concrete and steel columns of Example 5.

2.6.3 Description of the problem

Members with the characteristics defined in *Figure 49* and *Table 13* are analysed. In order to validate the results, the load bearing capacity of the members is determined and compared to the reference values presented in DIN EN1992-1-2 NA.

2.6.4 Models and results (see folder DIN6 4)

The same models of the previous example were used, but the *tem* files were modified and a new custom load function named “flood.fc” was introduced, in order to allow for a phase where the cross-section is heated without load for 512s until it reaches the target temperature, and another phase where the load is increased at constant temperature until the failure of the column.

One single beam element was used, which does not allow buckling of the columns to develop. This decision is motivated by the low slenderness of the columns that are proposed, which seems to indicate that this example has been designed with validation of the material laws in mind, more than the validation of a structural behaviour. The good match that will be observed between the calculated results and the reference results seems to confirm that this was indeed the case.

The results for the differences in the ultimate resistances obtained in static analyses performed by SAFIR and the reference results are presented in Table 16 and Table 17.

Table 16 – Ultimate resistance of the steel member in Example 6

Temperature θ	Reference force $N_{Rk,fi}$	Calculated force $N'_{Rk,fi}$	Deviation	
			$(N'_{Rk,fi,k} - N_{Rk,fi,k})$	$(N'_{Rk,fi,k} - N_{Rk,fi,k}) / N_{Rk,fi,k} \cdot 100$
°C	kN	kN	kN	%
20	-35.5	-35.5	0.0	0.00
200	-35.5	-35.5	0.0	0.00
400	-35.5	-35.5	0.0	0.00
600	-16.7	-16.7	0.0	0.00
800	-3.9	-3.9	0.0	0.00
Limits			± 0.5	± 3.00

Table 17 – Ultimate resistance of the concrete member in Example 6

Temperature θ	Reference force $N_{Rk,fi}$	Calculated force $N'_{Rk,fi}$	Deviation	
			$(N'_{Rk,fi,k} - N_{Rk,fi,k})$	$(N'_{Rk,fi,k} - N_{Rk,fi,k}) / N_{Rk,fi,k} \cdot 100$
°C	kN	kN	kN	%
20	-20	-20.0	0.0	0.00
200	-19	-19.0	0.0	0.00
400	-15	-15.0	0.0	0.00
600	-9	-9.0	0.0	0.00
800	-3	-3.0	0.0	0.00
Limits			± 0.5	± 3.00

2.6.5 Conclusions

A perfect agreement between the expected results and the ones obtained by SAFIR was found for all the cases considered, using the 2D BEAM elements.

Calculations were also performed using the TRUSS and the BEAM 3D elements, for the cases with 600°C, which returned the same (or virtually the same) results as for the BEAM 2D cases, for both steel and concrete.

2.7. Example 7 – Development of restraint stresses

2.7.1 Keywords

Thermal induced forces, steel, homogenous temperature, varying temperature

2.7.2 Objective

The goal of this example is to determine the thermal induced internal forces and stresses for a fixed-fixed steel beam, for two different temperature distributions: one constant and one that varies linearly on the depth of the cross-section.

2.7.3 Description of the problem

The members with the characteristics defined in Figure 50 and Table 18 are analysed. In order to validate the results, the values of the internal axial and bending forces and the stresses at the bottom of the cross-section are determined for the two temperature distributions and compared to the reference values presented in DIN EN1992-1-2 NA.

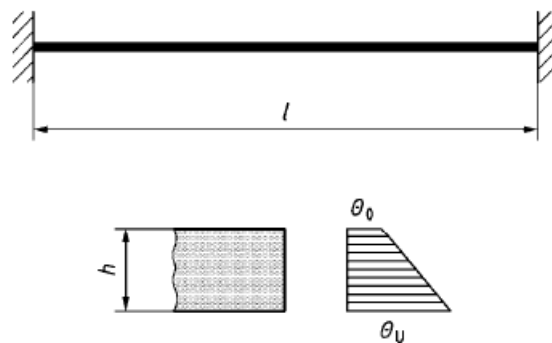


Figure 50 – Example 7: Fixed-fixed member and temperature distributions in the cross-section

Table 18 – Dimensions, material properties and boundary conditions for Example 7

Properties			Steel	
Dimensions l, h, b	mm		1000, 100, 100	
Stress-strain material law			EN 1993-1-2	
Yield strength f_y	N / mm ²		650 ^a	
Elastic modulus E_a (20°C)	N / mm ²		210 000	
Thermal expansion			EN 1993-1-2	
Temperature of the member	θ_o	°C	120	20
	θ_u	°C	120	220
a - Structural steel according to DIN EN 1993-1-1 using the notional yield f_y (20 ° C) = 650 N / mm ² (no high-strength steel) and the thermo-mechanical properties according to DIN EN 1993-1-2				

2.7.4 Models and results (see folder DIN7 4)

Two .tem files were created with 20 fibres of 5 mm depth equally distributed on the depth of the section. The temperature of 120°C was assigned to all fibres in the first file. In the second file, the temperature varied linearly from 25°C in fibre 1 to 215°C in Fibre 20.

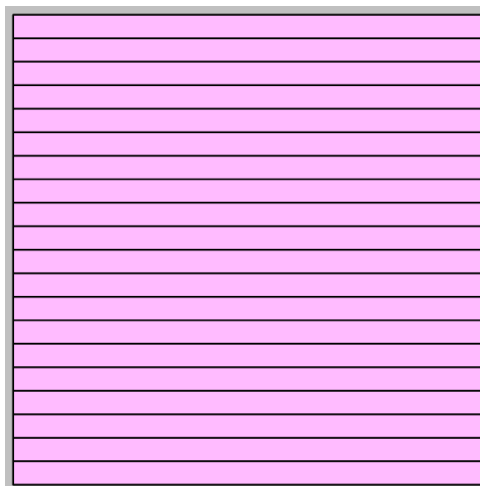


Figure 51 – Cross-section used for Example 7 (20 fibres)

A 2D mechanical model with 1 BEAM element was created and duplicated in order to be associated to the 2 different temperature distributions. STATIC analyses using a PURE_NR (pure Newton-Raphson) procedure, with a PRECISION of 10⁻³s and a time step of 1s were performed with the STEELEC3EN material. The results obtained are shown in Table 19.

Table 19 – Internal forces and stresses due to thermal expansion for Example 7

Temp.	Parameter		Reference	Calculated	Deviation	Limits
θ_0 θ_u	Desig.	Units	X	X'	$(X' - X) / X \cdot 100$	
°C					%	%
120 120	N_{zw}	kN	-2585	-2584.8	-0.01	± 1.00
	M_{zw}	kN.m	0	0	0.00	± 1.00
	σ_{zw}	N / mm ²	-258.5	-258	-0.19	± 5.00
20 220	N_{zw}	kN	-2511	-2510.6	-0.02	± 1.00
	M_{zw}	kN.m	-40.3	-40.207	-0.23	± 1.00
	σ_{zw}	N / mm ²	-479	-469	-2.09	± 5.00

2.7.5 Conclusions

A good agreement between the reference results and the ones obtained by SAFIR was found for the results for both the cases.

It has to be mentioned that the stresses were determined for the fibres at the bottom of the cross-section and hence their value do not correspond precisely to the value at the bottom edge, but to the centre of the fibre. This is the cause of the difference of 2% found for the 20|220 case. The difference for this case will be reduced if a thinner fibre is considered at the edge of the section. For instance, if a mesh with 200 fibres of equal size is considered, the stress determined by SAFIR at the bottom fibre is 478 N/mm², hence much closer to the 479 N/mm² presented in DIN.

2.8. Example 8 – Weakly reinforced concrete beam

2.8.1 Keywords

Fire resistance time, weakly reinforced concrete beam, ISO fire curve

2.8.2 Objective

Example 8 deals with a weakly reinforced concrete beam with a uniform distributed load that is subjected to the standard fire on three sides. The goal is to determine the requested area for the two steel rebars in order to provide a fire resistance of 90 minutes to the beam.

2.8.3 Description of the problem

The member with the characteristics defined in Figure 52 and Table 20 is analysed. The required value for the steel area to ensure that the beam reaches 90 min of resistance when subjected to an ISO fire is determined and compared to the reference value presented in DIN EN1992-1-2 NA.

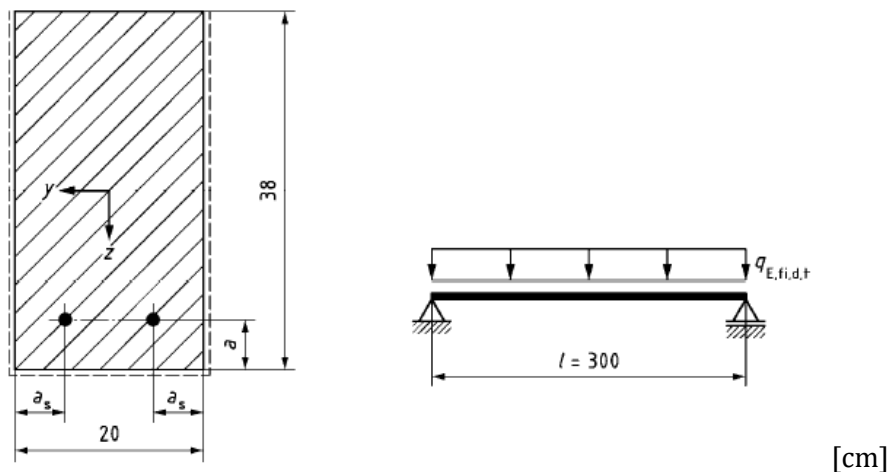


Figure 52 – Example 8: Cross-section and configuration of the weekly reinforced concrete beam

Table 20 – Dimensions, material properties and boundary conditions for Example 8

Fire resistance category			R90
Dimensions	l, b, h	mm	3000, 200, 380
Spacing	a, a_s	mm	45, 55
Loads	$q_{E,fi,d,t}$	kN/m	29
Concrete C20/25	$f_c(20^\circ\text{C})$	N/mm ²	20
Moisture content (by mass)	w	%	3
Steel B500	$f_y(20^\circ\text{C})$	N/mm ²	500
Stress-strain material law	Concrete ^a		EN 1992-1-2
	Rebars ^b		
Fire exposure	ISO 834 (three sides)		EN 1991-1-2
Coefficient of convection	α_c	W/(m ² .K)	25
Emissivity	ϵ_m		0.7
Thermal and physical material properties	Concrete	$\lambda, \rho, c_p, \epsilon_{th,c}$	EN 1992-1-2
	Steel	$\lambda_a, \rho, c_a, \epsilon_{th,s}$	EN 1994-1-2

^a – with predominantly siliceous aggregates and density $\rho = 2400 \text{ kg/m}^3$
^b – class N, hot-rolled

2.8.4 Models and results (see folder DIN8 4)

Different models of the section were created, by changing the area of the two steel bars from one model to another (see Figure 53). The ISO fire curve was applied on 3 sides of the section while the upper side was adiabatic.

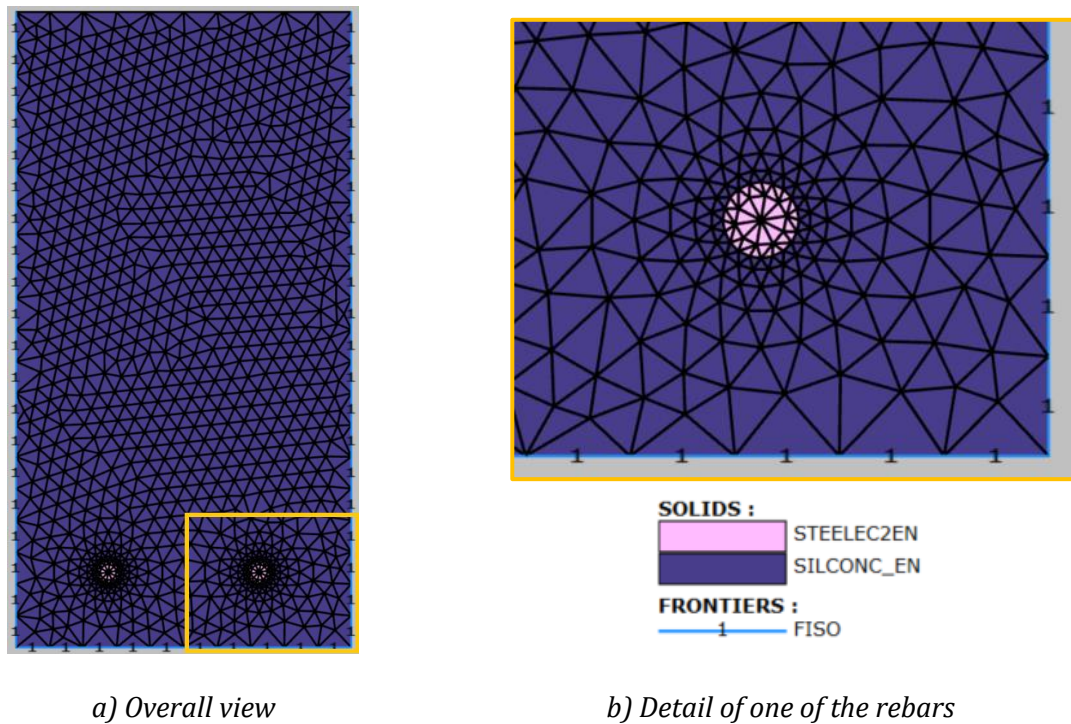


Figure 53 – Example of one of the thermal models of the cross-section tested for Example 8

The whole length of the beam was modelled with 20 2D BEAM finite elements of equal length (see Figure 54).

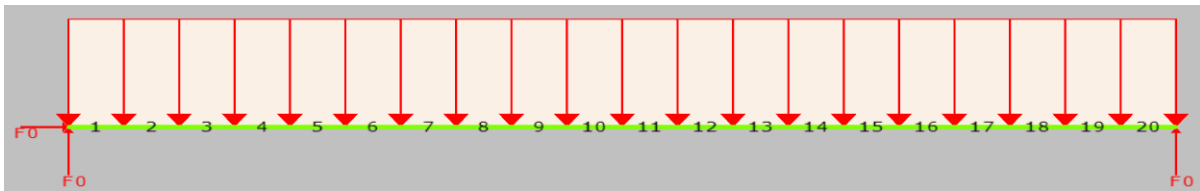


Figure 54 – Structural model of the beam (20 BEAM elements of equal sizes)

Steel was modelled by the material STEELEC2EN, with the fabrication process HOTROLLED and with the ductility class B (no mention to the ductility class is given in DIN but this was found to be the one resulting in better approximations to the results in DIN).

Concrete was modelled by the material SILCONC_EN. In thermal analysis, the upper limit for the thermal conductivity, found in clause 3.3.3 of EN1992-1-2, was considered, since this is this one recommended by Eurocode and that led to better approximations to the results in DIN.

The calculations performed were DYNAMIC and used the PURE_NR (pure Newton-Raphson) procedure. The initial time step was set to 1s, the maximum time step to 60s, the PRECISION to 10E-3s, and the COMEBACK to 0.01s.

The fire resistance times obtained in the mechanical analyses, corresponding to the last converged time step, were observed for each section used. It was found that a diameter for each of the two rebars of 14.47 mm is required to obtain a fire resistance of 90 minutes (with a margin of error of 0.5 min), which corresponds to a total steel reinforcement area of 3.29 cm².

The temperature in the rebars and the fire resistance times obtained for the different iterations made are shown in Figure 55.

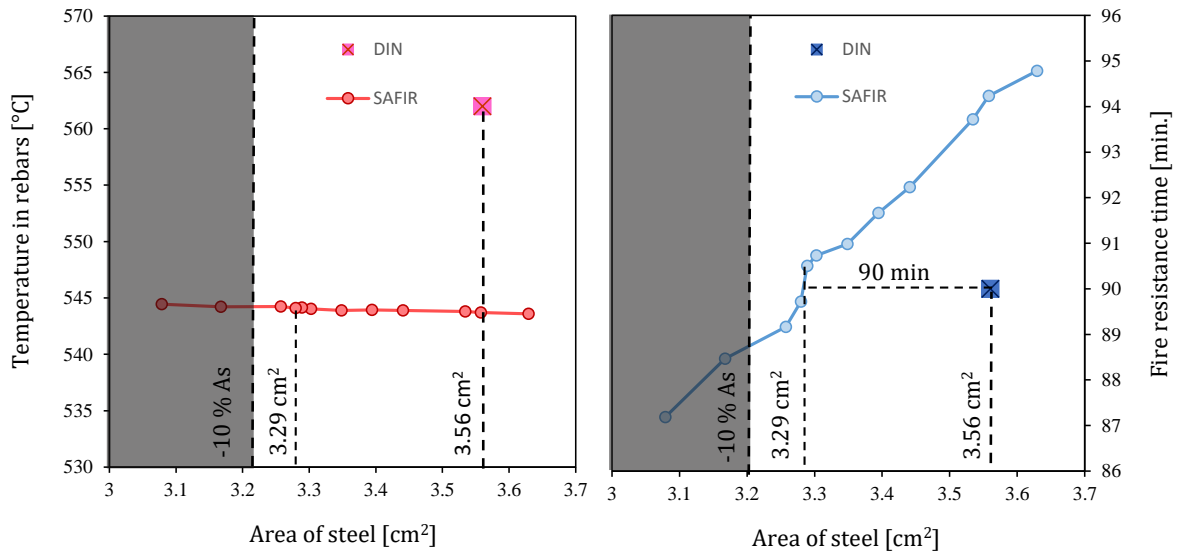


Figure 55 – Evolution of the temperature at the centre of the rebars and of the fire resistance with the steel area

The temperature distribution after 90 minutes, in the section with $A'_s = 3.29 \text{ cm}^2$, is shown in Figure 56.

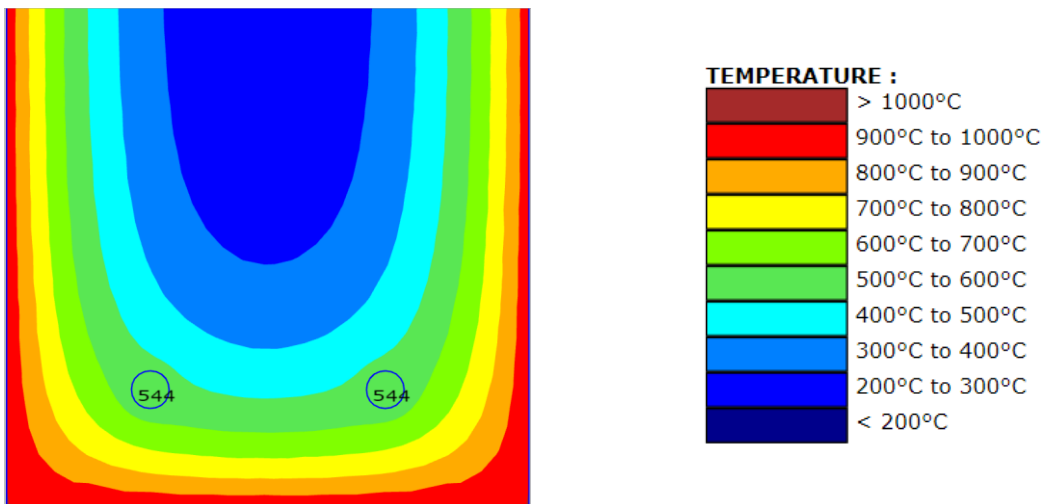


Figure 56 – Temperatures determined by SAFIR for $t = 90 \text{ min}$, for Example 8, with two rebars of 14.47mm (bottom part of the model)

Figure 57 shows the evolution of the vertical displacement at mid-span of the beam. The vertical displacement at the last converged time is 106 mm, corresponding to $1/28.3$. The horizontal inward displacement on the right hand support is 28.1 mm for the same time instant.

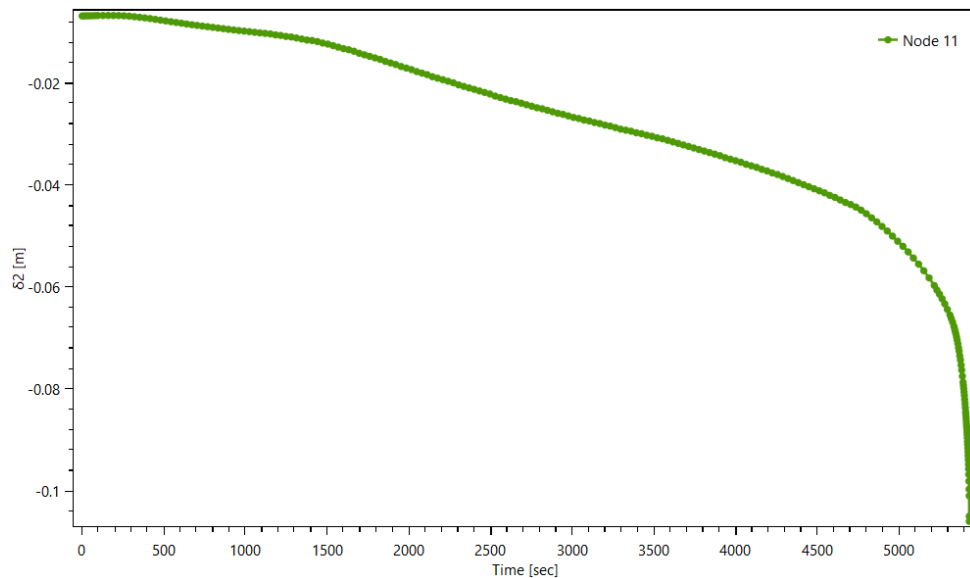


Figure 57 – Vertical displacement vs. time at mid-span of the beam obtained by SAFIR

The results obtained with SAFIR, as well as the reference values of DIN EN1992-1-2 NA, are summarized in Table 21.

Comments on the results obtained will be given at the last part of this example.

Table 21 – Necessary area of steel to resist an ISO fire for 90 min, for the weekly reinforced concrete beam in Example 8

Fire resistance class	Temperature in the rebars for t = 90 min		Area of the steel rebars			
	Reference	Calculated	Reference	Calculated	Deviation	Limit
	T	T'	A_s	A'_s	$(A'_s - A_s) / A_s \cdot 100$	
°C	°C	cm ²	cm ²	%	%	
R90	562	544	3.56	3.29	-7.61	± 10.00

2.8.5 Analysis of the influence of different parameters in the structural analysis

An analysis of the sensibility of the results to different parameters is done, which will provide indications on the influence of the type of analysis, on the minimum value of the time step or the minimum number of BEAM elements necessary to accurately simulate the mechanical behaviour of the beam, and to confirm that the solution converges to a value as the mesh is refined.

The thermal model with the area of steel of 3.29 cm² mentioned above was used in all the analyses.

2.8.5.1 Influence of the type of analysis (see folder DIN8_5_1)

To study the influence of the type of analysis (static or dynamic) and the type of procedure (pure Newton-Raphson or approximated Newton-Raphson), the cases presented in Table 22 were tested. The same mechanical model with 20 BEAM elements was used. Both procedures were

tested in a STATIC and in a DYNAMIC analysis. For the DYNAMIC analyses, three values for the mass were used: 0 kg/m; 190 kg/m (the mass of the beam); and 2090 kg/m (the mass of the beam plus the mass of the gravity load).

The results obtained allow to conclude that, for the current example, the type of analysis and type of procedure chosen don't affect the results, regardless of the value given for the MASS (in DYNAMIC analyses).

Table 22 – Fire resistance times obtained with different analysis options, for Example 8

Case	Type of analysis		MASS	Fire resistance time
Name	Type	Procedure	kg/m	min
DIN8_5_1()				
a	STATIC	PURE_NR	-	90.5
b		APPR_NR	-	90.5
c	DYNAMIC	PURE_NR	0	90.5
d*			190	90.5
e			2090	90.5
f		APPR_NR	0	90.5
g			190	90.5
h			2090	90.5

*same case as the one tested before in 2.8.4

2.8.5.2. Influence of the time step (see folder DIN8_5_2)

To study the influence of the time step on the results, the same model was used, and values of the time step equal to 5, 10, 30, 60, 120, 300 and 600 s were tested. Two types of analysis, one STATIC and one DYNAMIC with the MASS of 190 kg/m, were performed. The results are shown in Table 23.

Table 23 – Fire resistance times obtained with different time steps, for the two types of analysis, for Example 8

Case	STATIC analysis		DYNAMIC analysis		
	Time step	Fire resistance time	Initial time step	Maximum time step	Fire resistance time
	s	min	s	s	min
a	5	90.5	5	30	90.5
b	10	90.5	5	60	90.5
c	30	90.5	5	120	90.5
d	60	90.5	5	300	90.5
e	120	90.5	5	600	90.5
f	300	90.5	30	600	90.5
g	450	90.5	60	600	90.5
h	600	90.5	300	600	90.5
i	1200	90.5	600	600	90.5

The change in the value of the time step in the mechanical analysis didn't produce any effects in this simple structure. This may not be the case in more complex structures.

2.8.5.3. Influence of the number of elements (see folder DIN8_5_3)

To assess the influence of the refinement of the mesh of the mechanical model on the results, 7 different meshes - with 2, 4, 6, 8, 12, 16, and 20 BEAM elements of equal sizes - were analysed, considering the assumptions in 2.8.4.

The results for the fire resistance time obtained with each model are presented in Figure 58. It is seen that results converge to the value of 90.5 minutes as the mesh is refined.

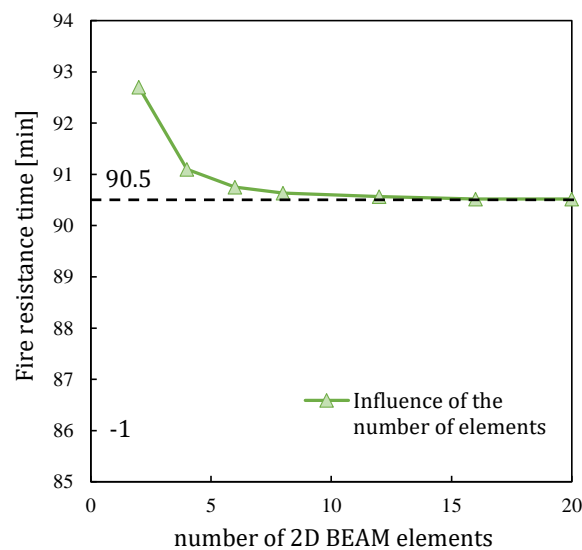


Figure 58 – Fire resistance times obtained with different meshes for the mechanical model, for Example 8

It has yet to be mentioned that the bending moment distribution is such that the whole central part of the beam is subjected to a bending moment that is very close to the maximum bending moment. The convergence of the solution as a function of the number of elements might be slower in case of peaks in the bending moment distribution (with a point load, for example).

2.8.6 Discussion and conclusions

The temperature determined by SAFIR in the rebars is 544°C and hence a little bit lower (around 3%) than the 562°C mentioned in DIN. This is not related to the difference in the size of the rebars, as it is shown in Figure 55 that for the range of steel reinforcement areas analysed, which covers the area of 3.56 cm² preconized in DIN, the temperature does not vary significantly.

Nevertheless, a deviation of 7.61% for the necessary area is still well inside the boundaries provided by the DIN, and it can be at least partly justified by the differences found for the temperature on the rebars. In fact, if the model with the reference area of 3.56 cm² is considered, the structural analysis in SAFIR will fail to converge at the time instant $t = 94.2\text{min}$, time that corresponds approximately to having the reference temperature of 562°C in the rebars, as can be seen in Figure 59.

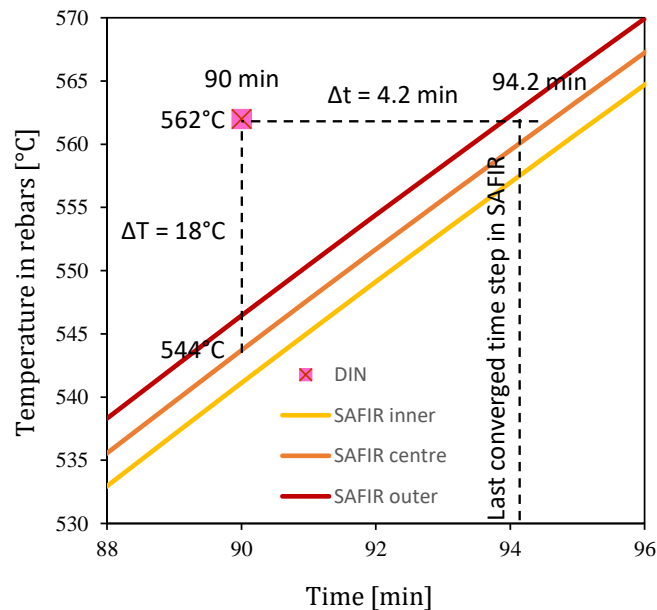


Figure 59 – Evolution of the temperature at the centre, innermost and outermost points of the rebars, for the SAFIR model with the reference area $A_s = 3.56 \text{ cm}^2$

One other aspect that should be brought to discussion is the lack of definition in DIN regarding the criteria for the moment where the beam fails. All the results above were presented considering that the time of failure is the last converged time step in SAFIR. However, according to [9], the last 4 examples (Examples 8 to 11), which simulate fire tests, are based on results from approved numerical tools. There is no indication in DIN about the criteria used to determine the time of failure from these simulations with approved numerical tools. Therefore, it is possible that the observed discrepancies come from a different definition of failure.

That said, if the criteria presented in the European standard for fire testing [6] is adopted, two limits should be considered: a limiting deflection and a limiting deflection rate. According to the standard, the first has a value of 67 mm for this example, based on the geometric characteristics of the beam, while the second has a value of 3 mm/min.

Following that criteria, and assuming that the failure time corresponds to the first of these two limits to be reached, a section with 3.49 mm^2 will lead to a fire resistance of 90 min (if the rate of deflection is determined by a first-order backward difference method computed for every minute) as seen in Figure 60. This value represents a deviation of only 2.04% to the area suggested by the DIN.

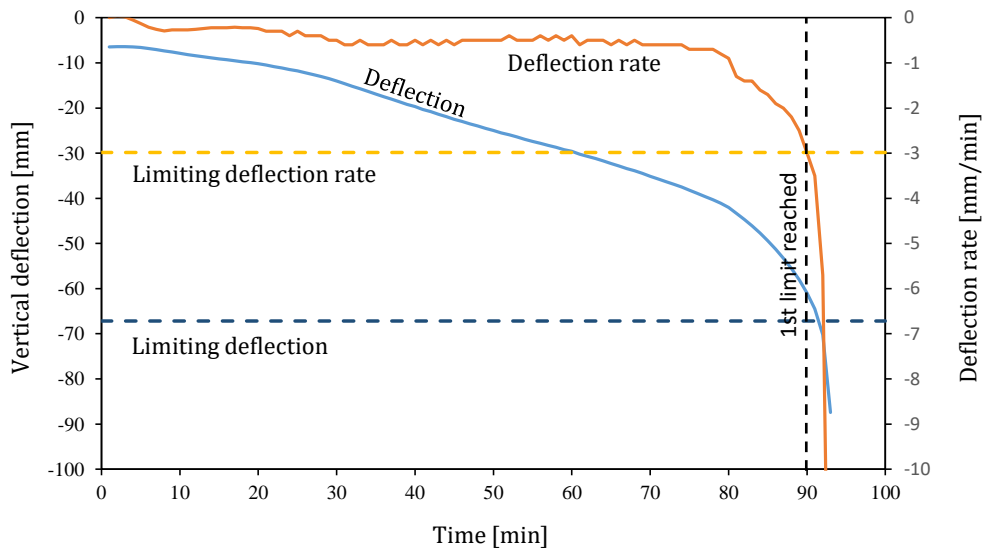


Figure 60 – Deflection and deflection rate vs. time obtained with SAFIR for the section with $A's = 3.49 \text{ cm}^2$, with limits for the loadbearing capacity according to the criteria in EN 1363-1 [6]

From the parametric analysis it can be concluded that for the mechanical analyses of simple structures like the one herein present, the choice regarding the type of analysis or regarding the time step used is not relevant, and that for such a structure the results for the fire resistance converge to a given value as the mesh is refined.

2.9. Example 9 – Heavily reinforced concrete beam

2.9.1 Keywords

Fire resistance time, heavily reinforced concrete beam, ISO fire curve

2.9.2 Objective

Example 9 deals with a concrete beam with the same characteristics as the one in Example 8, but subjected to a higher load and reinforced with 6 rebars. The goal is the same, to determine the required area of the steel rebars that leads to a fire resistance to the ISO fire of 90 minutes.

2.9.3 Description of the problem

The member with the characteristics defined in Figure 61 and Table 24 is analysed. In order to validate the results, the required steel area for the beam reaching 90 min of resistance when subjected to an ISO fire is determined and compared to the reference value presented in the DIN EN1992-1-2 NA.

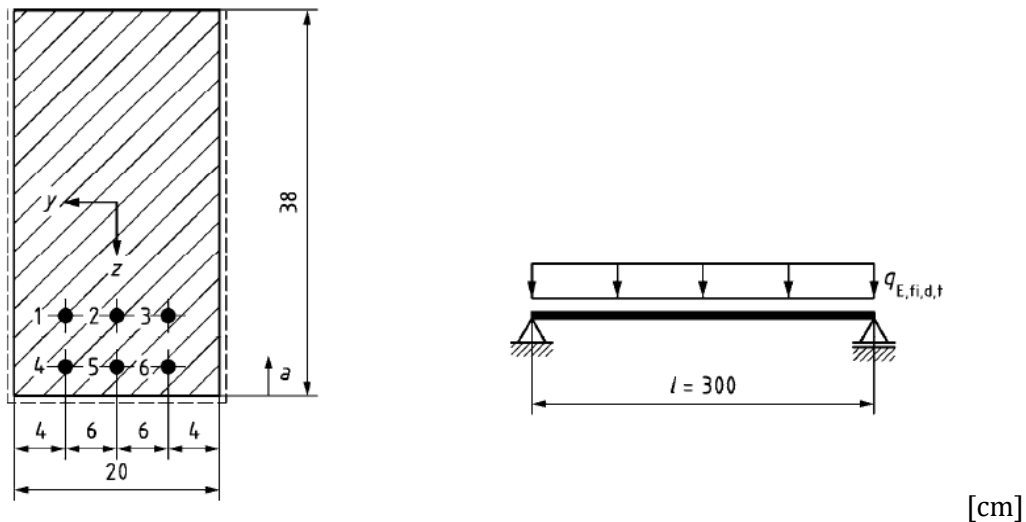


Figure 61 – Example 9: Cross-section and configuration of the strongly reinforced concrete beam

Table 24 – Dimensions, material properties and boundary conditions for Example 9

Properties for reinforced concrete beam (strongly reinforced)			R90
Dimensions	l, b, h	mm	3000, 200, 380
Spacings	$a_{1,2,3}$	mm	70
	$a_{4,5,6}$	mm	40
Loads	$q_{E,fi,d,t}$	kN/m	62.9
Concrete C20/25 (3% humidity by mass)	$f_{ck}(20^{\circ}C)$	N/mm ²	20
Steel B500	$f_{yk}(20^{\circ}C)$	N/mm ²	500
Stress-strain material law	Concrete ^a		EN 1992-1-2
	Rebars ^b		
Fire exposure	ISO 834 (three sides)		EN 1991-1-2
Heat transfer coefficient	α_c	W / (m ² .K)	25
Emissivity	ϵ_m		0.7
Thermal and physical material values	Concrete	$\lambda, \rho, c_p, \epsilon_{th,c}$	EN 1992-1-2
	Steel	$\lambda_a, \rho, c_a, \epsilon_{th,s}$	EN 1994-1-2
^a – with predominantly siliceous aggregates and density $\rho = 2400 \text{ kg/m}^3$			
^b – class N, hot-rolled			

2.9.4 Models and results (see folder DIN9_4)

Similarly to the previous example, thermal models of the section were created with different diameters of the rebars, and the resulting temperature fields were used on a structural 2D model with 20 BEAM elements of equal sizes. The fire resistance time of each model was observed, until one gave a fire resistance time of 90 min (with a margin of error of 0.5 min).

The calculations performed were DYNAMIC and used the PURE_NR (pure Newton-Raphson) procedure. The structural model was defined with an initial time step of 1s, a maximum time step of 60s, a PRECISION of 10E-3s and a COMEBACK of 0.01s.

The fabrication process and the ductility class for the STEELEC2EN material were set as HOTROLLED and CLASS_B, respectively, and the concrete as SILCONC_EN. In the thermal model (see Figure 62), the thermal conductivity for the concrete was set to follow the upper limit according to EN1992-1-2.

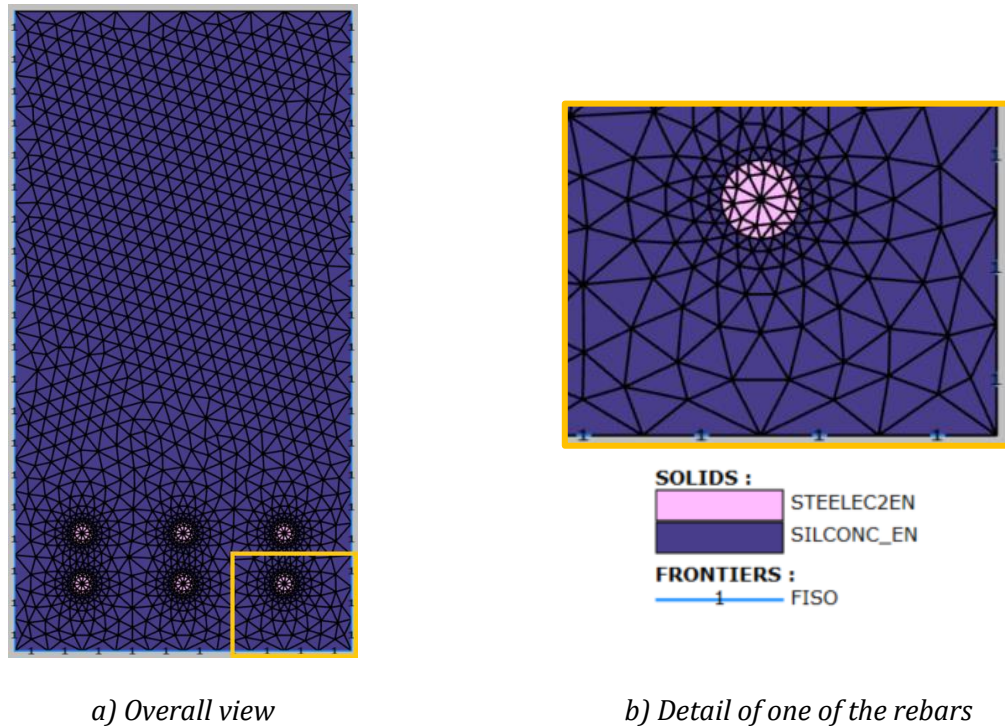


Figure 62 – Example of one of the thermal models of the cross-section tested for Example 9

The required reinforcement for a 90 minutes fire resistance corresponds to a diameter $\Phi = 13.2$ mm for the six rebars, which gives a total steel area $A'_s = 8.21$ cm².

The temperature in the corner rebars and the fire resistance times obtained for the different iterations made are shown in Figure 63. The temperature in the rebars for all the models was taken in the left corner rebar.

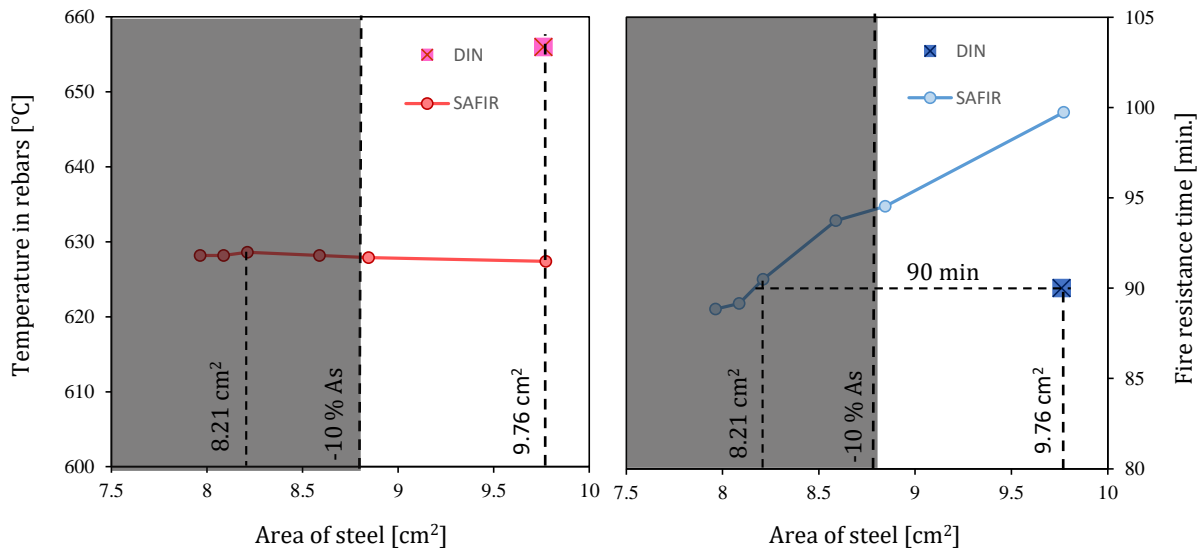


Figure 63 – Temperature at the centre of the corner rebars and fire resistance times obtained with the different models tested, for Example 9

The temperature distribution after 90 min is shown in Figure 64 for the section with $A'_s = 8.21 \text{ cm}^2$.

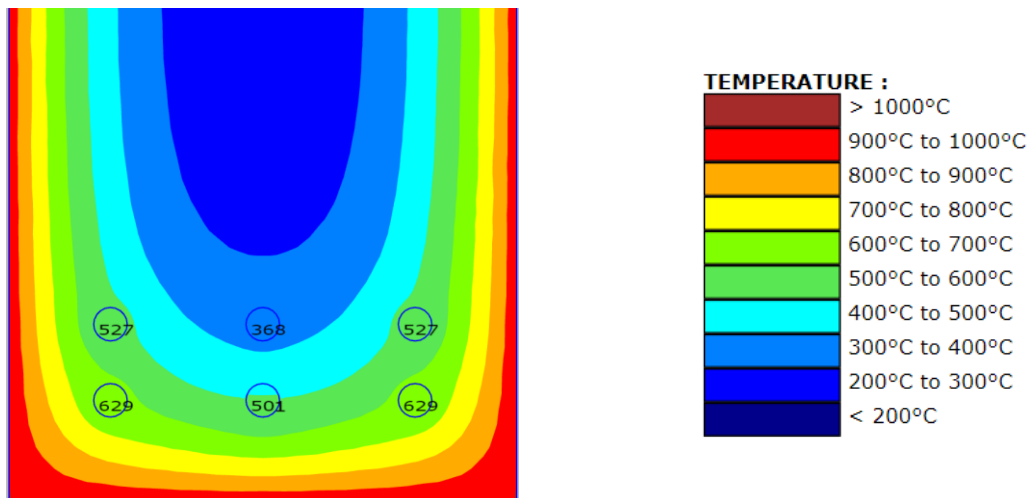


Figure 64 – Temperatures determined by SAFIR for $t = 90 \text{ min}$, for Example 9, with six rebars of 13.2mm (bottom part of the model)

Figure 65 shows the evolution of the vertical displacement at mid-span of the beam. The vertical displacement at the last converged time step is 81 mm, corresponding to $l/37.5$. The horizontal inward displacement at the support on the right is 8.3 mm for the same time instant.

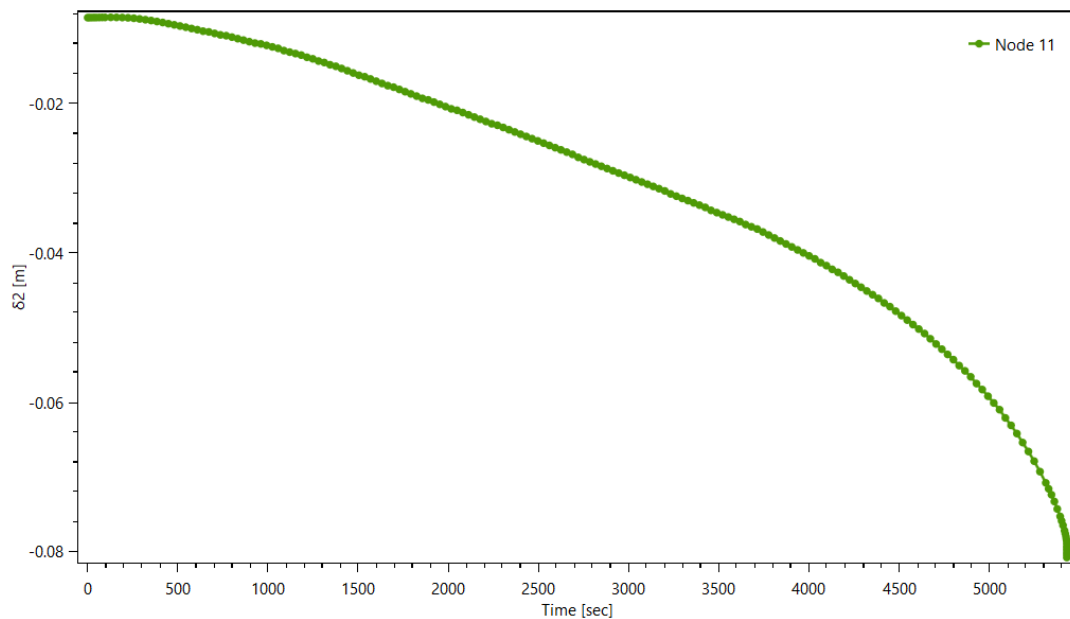


Figure 65 – Time vs vertical displacement of the node at mid-span of the beam obtained by SAFIR, for Example 9

The results obtained with SAFIR and the deviation from DIN EN1992-1-2 NA are summarized in Table 25.

Table 25 – Necessary area of steel to resist an ISO fire for 90 min, for the heavily reinforced concrete beam in Example 9

Fire resistance class	Temperature in the corner rebars for t = 90 min		Area of the steel rebars			
	Reference	Calculated	Reference	Calculated	Deviation	Limit
	T	T'	A _s	A' _s	(A' _s - A _s) / A _s .100	
	°C	°C	cm ²	cm ²	%	%
R90	656	629	9.76	8.21	-15.9	± 10.00

2.9.5 Discussion and conclusions

As for the previous example, the temperatures determined in the rebars after 90 minutes are lower than the ones provided by the DIN. As a consequence, the amount of steel required to obtain the 90 min resistance is less than the reference value, but, in this case, the difference exceeds the acceptable tolerance by 5.9%.

It has to be noted that other software produce results similar to SAFIR (see Figure 66). For example, with INFOGRAPH [7], the reference reinforcement area of 9.76 cm² yields a fire resistance time of 96 min, which is also considerably larger than the expected 90 min. With FRILO [8], a steel reinforcement area of 8.57 cm² leads to a fire resistance of 93 min, very close to the 93.7 min obtained by SAFIR when considering 8.59 cm².

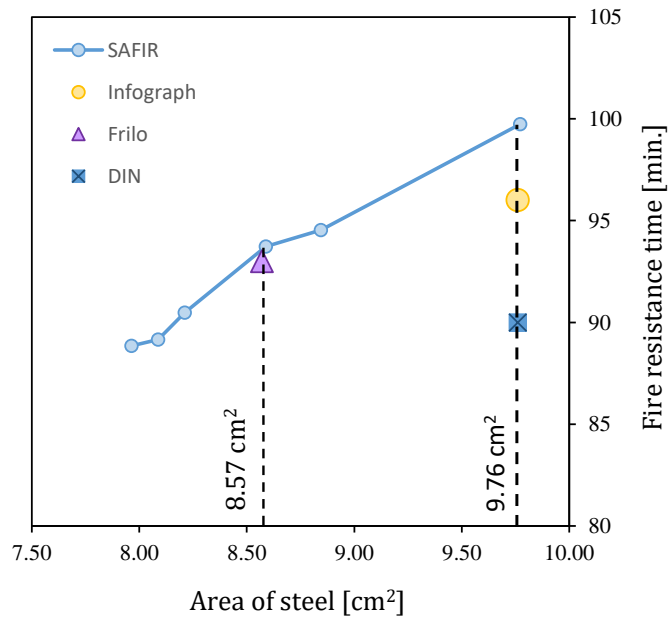


Figure 66 – Comparison between fire resistance times obtained with SAFIR, different Software and the one presented in DIN, for Example 9

Considering the criteria in the European standard for fire testing [6] and assuming that the failure time corresponds to the first of the two limits - limiting deflection and limiting deflection rate - to be reached, a section with a steel reinforcement area of 8.84 mm² will lead to a fire resistance of 90 min, as seen in Figure 67. This value represents a deviation of 9.38% to the area suggested by the DIN, which is still relatively big but that falls inside the 10% of deviation allowed.

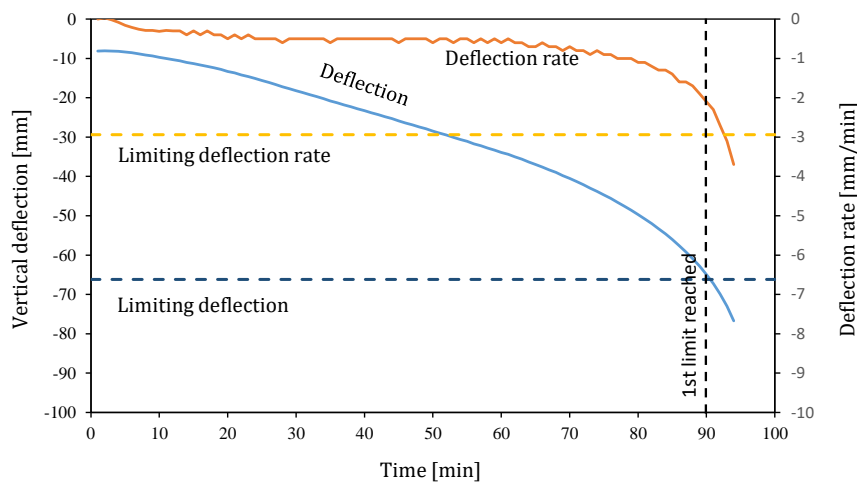


Figure 67 – Deflection and deflection rate vs. time obtained with SAFIR for the section with A's = 8.84 cm², with limits for the loadbearing capacity according to the criteria in EN 1363-1 [6]

As pointed out before, the last 4 examples in DIN (this one included) are based on results from approved numerical tools. Despite being referred as 'approved tools' in [9] and [10], there is no apparent proof of the accuracy of these results, nor is there any indications on the considerations and assumptions taken in the analyses that produced them. For instance, it is not

clear what should be the values used for the thermal conductivity. A clear definition of failure, and the criteria used to determine the failure time, is also missing. Additionally, the fact that other software obtained identical results to the ones found here, is certainly something that should not be neglected.

This is why the authors of this report consider that the excessive deviation with respect to the reference value of the DIN does not invalidate the ability of SAFIR to model the behavior of concrete beams subjected to fire. Comparison with 2 other independent software yielding similar results when using the same hypotheses appears to be of greater significance.

2.10. Example 10 – Reinforced concrete beam-column

2.10.1 Keywords

Fire resistance time, displacements, bending moments, beam-column, reinforced concrete, ISO fire curve

2.10.2 Objective

Example 10 deals with a reinforced concrete beam-column loaded with a horizontal distributed load and a vertical load with an eccentricity, and subjected to fire on all sides. The goal is to determine the failure time as well as one displacement and one reaction after 90 minutes of fire.

2.10.3 Description of the problem

The member with the characteristics defined in Figure 68 and Table 26 is analysed. In order to validate the results, the time when the member collapses as well as the horizontal displacement at the top and the bending moment at the support for 90 minutes of an ISO fire are calculated and compared to the reference values presented in DIN EN1992-1-2 NA.

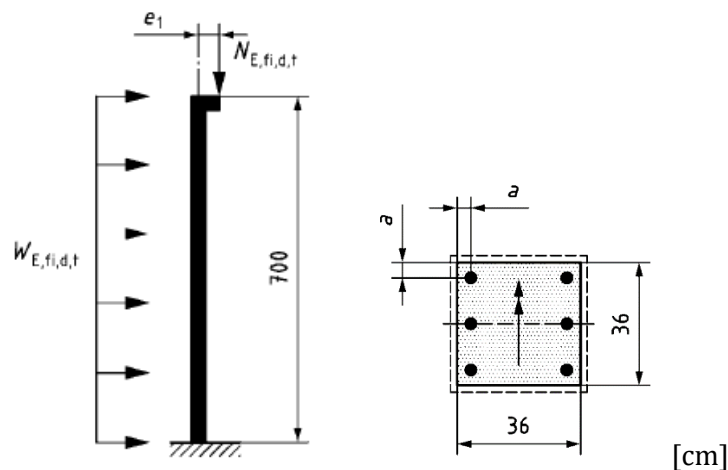


Figure 68 – Example 10: Cross-section and configuration of the reinforced concrete beam-column

Table 26 – Dimensions, material properties and boundary conditions for Example 10

Properties	R90
------------	-----

Dimensions	l, b, h	mm	7000, 360, 360
Load eccentricity in fire	e_1	mm	35
Spacing	a	mm	55
Loads	$N_{E,fi,d,t}$	kN	79
	$W_{E,fi,d,t}$	kN/m	1.74
Concrete C20/25 (3% humidity by mass)	$f_c(20^\circ\text{C})$	N/mm ²	20
Steel B500	$f_y(20^\circ\text{C})$	N/mm ²	500
Stress-strain material law	Concrete ^a		EN 1992-1-2
	Rebars ^b		
Fire exposure	ISO 834 (four sides)		EN 1991-1-2
Heat transfer coefficient	α_c	W / (m ² .K)	25
Emissivity	ϵ_m		0.7
Thermal and physical material values	Concrete	$\lambda, \rho, c_p, \epsilon_{th,c}$	EN 1992-1-2
	Steel	$\lambda_a, \rho, c_a, \epsilon_{th,s}$	EN 1994-1-2

^a – with predominantly siliceous aggregates and density $\rho = 2400 \text{ kg/m}^3$
^b – class N, hot-rolled

2.10.4 Models and results (see folder DIN10 4)

The section was modelled with 3566 triangular finite elements (see Figure 69). It has to be noted that 3 bars are on the compression side and 3 bars are on the tension side, in the section (no bar at the neutral axis).

The structural model was made of 20 BEAM finite elements with equal sizes. A fictitious 3.5 cm long rigid element was used to apply the vertical load with an eccentricity, see Figure 70.

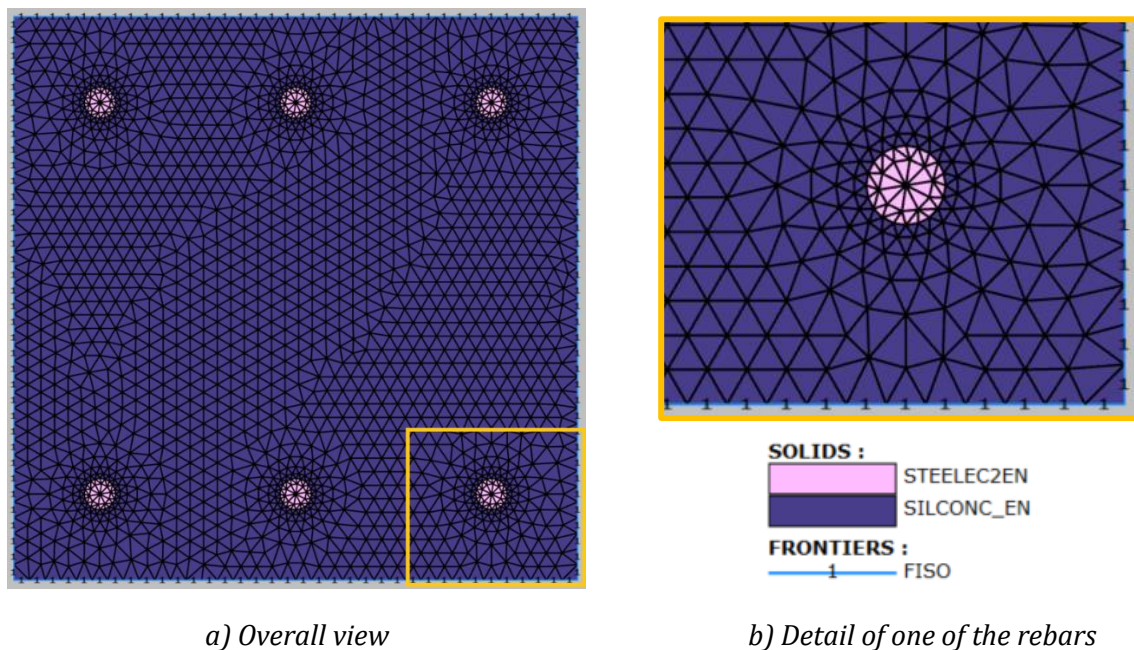
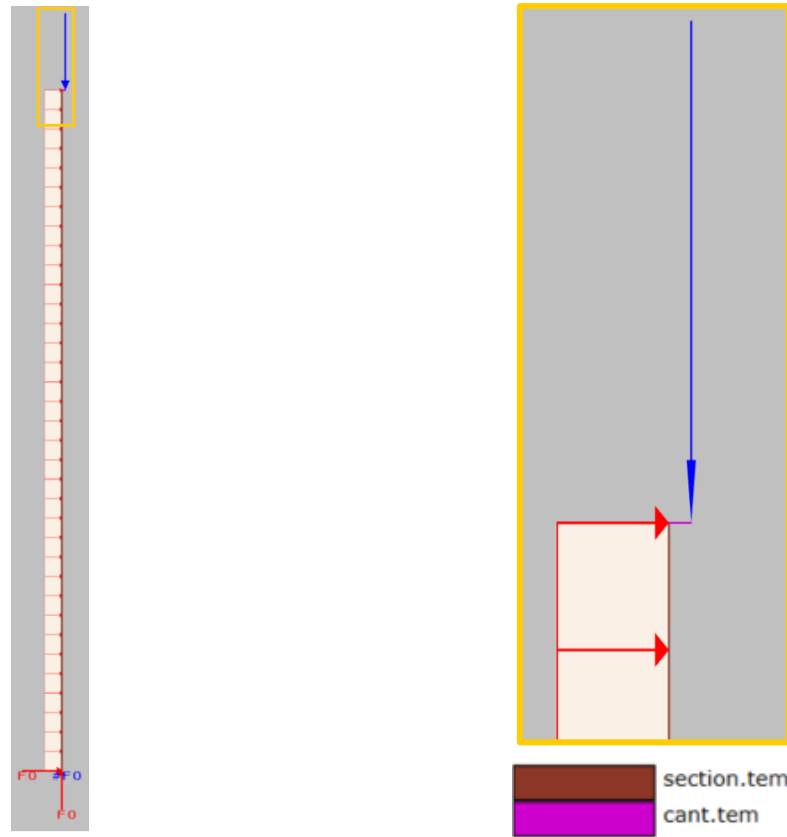


Figure 69 – Thermal model of the cross-section for Example 10



a) Overall view

b) Detail of the load eccentricity

Figure 70 – Structural model of the column for Example 10 (20 BEAM elements with equal sizes)

The calculations performed were STATIC and used the PURE_NR (pure Newton-Raphson) procedure. The structural model was defined with a PRECISION of 10E-3s, a COMEBACK of 1s, with a time step of 60s, and with the materials SILCONC_EN and STEELEC2EN.

The temperature distribution for t = 90 minutes is presented in Figure 71.

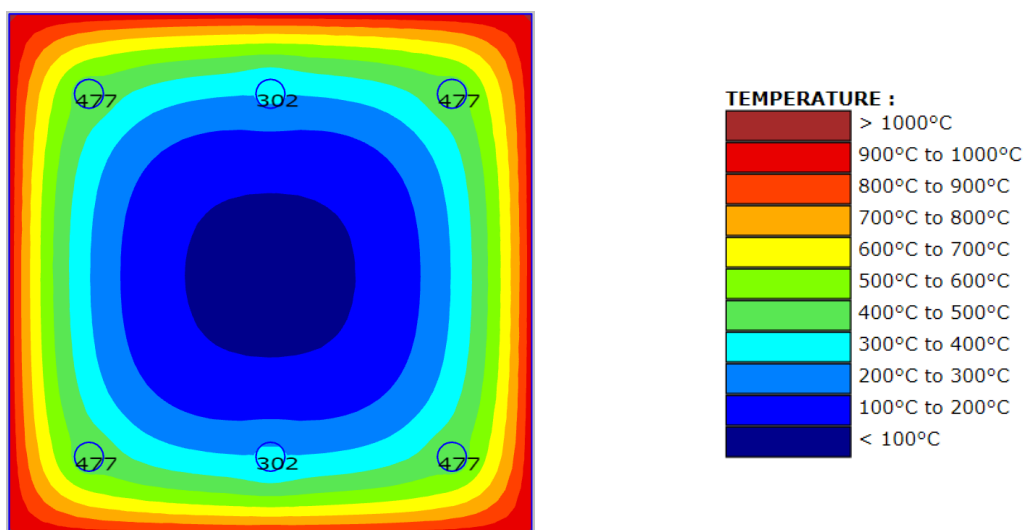


Figure 71 – Temperature distribution in SAFIR for Example 10, for $t = 90$ min

Figure 72 shows the evolution of the horizontal displacement at the top of the column. The horizontal displacement of the last converged time is 525 mm, corresponding to $l / 13.3$.

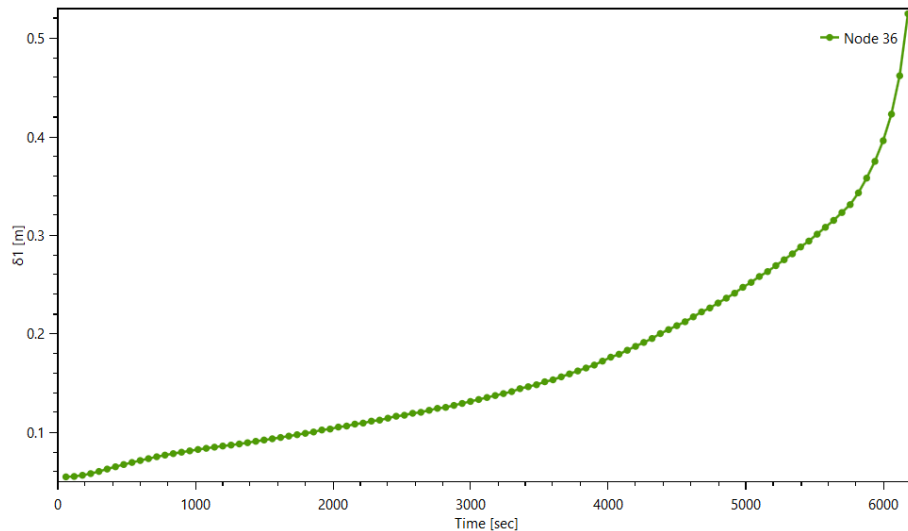


Figure 72 – Horizontal displacement vs. time for Example 10, for the node at mid-length of the column

The deviations from the DIN EN1992-1-2 NA are found in Table 27. The failure time instant considered was the last converged time step.

Table 27 – Failure time, horizontal displacement and bending moment for Example 10

Parameter			Reference	Calculated	Deviation	Limit	
			X	X'	$(X' - X) / X \cdot 100$		
					%		
Failure time t_u			min	93	103	10.75	± 3.00
For $t = 90$ min	Temp. in rebars	corners	°C	502	477	-4.98	-
		middle	°C	319	302	-5.33	-
	Hor. displacement ω_z at top of the column		mm	381	288	-24.41	± 15.00
	Moment $M_{E,fi,d}$ at the bottom of the column		kN.m	75.5	67.9	-10.07	± 5.00

2.10.1 Discussion and conclusions

Again, the temperatures determined by SAFIR for the rebars are lower than the ones provided by the DIN. For the rebars at the corners, a difference of -4.98% was found. This leads to a resistance time of 103 minutes and to a difference of 10.75% to the reference result, which is

considerably bigger than the allowed deviation of 3%. This is, at least, if failure is declared at the last converged time.

For the loadbearing criteria in the standard for experimental testing EN 1363-1, the criteria are different for two different situations: vertically and flexural loaded elements. Both situations will be considered here, because the lateral displacements play a major role on the deformation of the column, due to the horizontal load and to the eccentricity of the compression load.

As seen in Figure 73, the vertical elongation and vertical elongation rates don't get close to the limits for the contraction provided in EN1363-1 for vertically loaded elements, whereas a value of 98 minutes can be obtained based on the horizontal deflection allowed for flexural loaded elements. This corresponds to a difference of 5.38% compared to the reference time of 93 min.

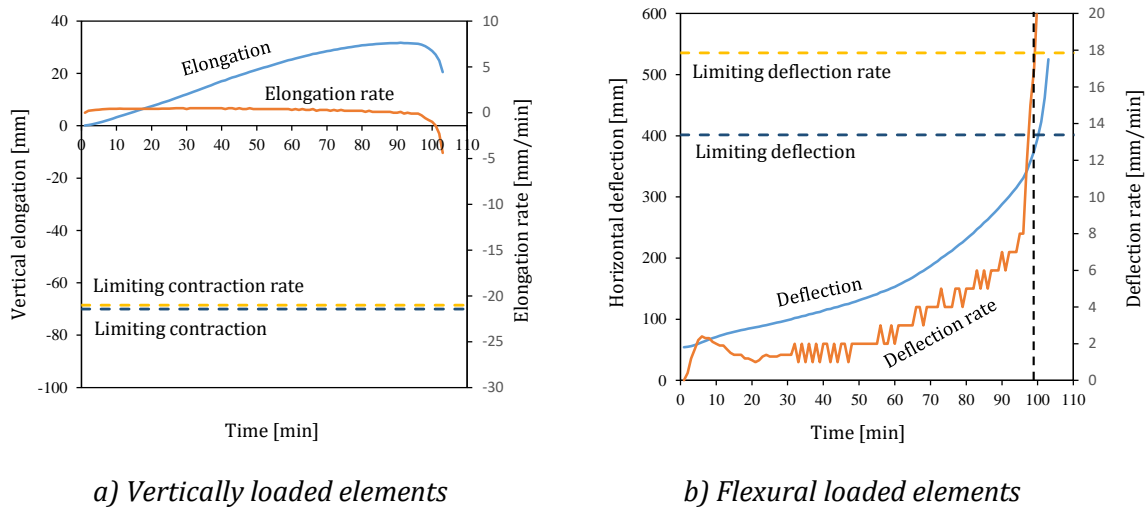


Figure 73 –Deflection and deflection rate vs. time obtained with SAFIR for the top node of the column, with limits for the loadbearing capacity according to the criteria in EN 1363-1 [6]

Regarding the horizontal displacement at the top and the bending moment at the bottom of the column for $t = 90$ min, the values calculated are lower than the limits defined by DIN. If the values calculated by SAFIR at $t = 98$ min (time of failure according to the EN1363-1 criteria) are considered, the horizontal displacement $w_z = 358$ mm and the bending moment $M_{E,fi,Ed} = 72,9$ kN.m fall well inside the limits provided of 15% and 10%, showing differences of -6.04% and -3.44%, respectively.

Other software found similar results to the ones presented in Table 27, and suggested that the temperatures mentioned in the DIN correspond to the ones obtained if the rebars are not present in the model of the cross-section. For INFOGRAPH [7] as well as for MBAEC [11], the results are closer to the ones from DIN when the thermal analysis is performed for an identical cross-section with only concrete.

The same was done with SAFIR, i.e. a thermal analysis was performed in a pure concrete section (the bars are of course present in the structural analysis). This leads to the results presented in Figure 74, Figure 80 and Table 28, in which the failure time, the horizontal displacement at the top and the bending moment at the bottom for $t = 90$ min, fall inside the stipulated boundaries.

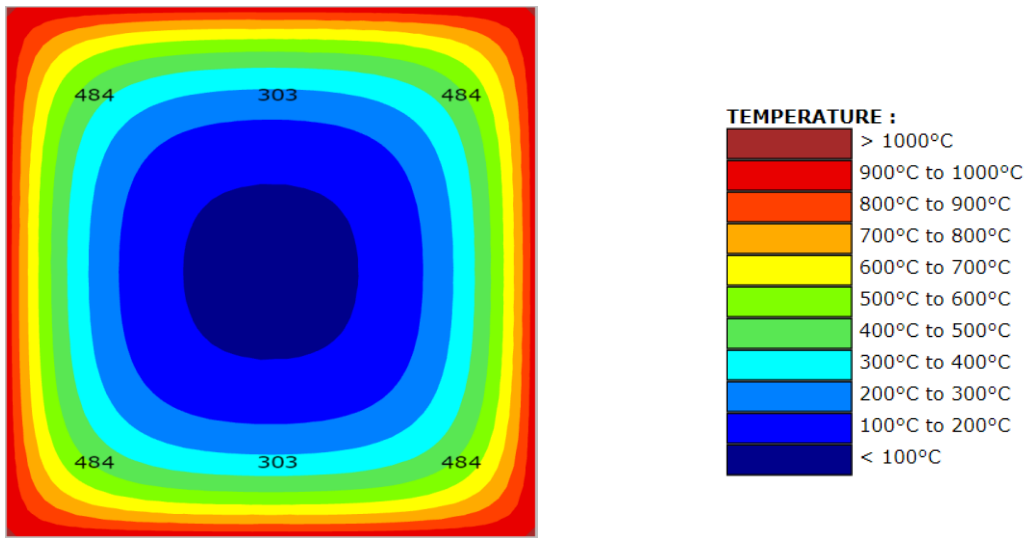


Figure 74 – Temperature distribution in SAFIR for Example 10, for $t = 90$ min, considering the cross-section with only concrete

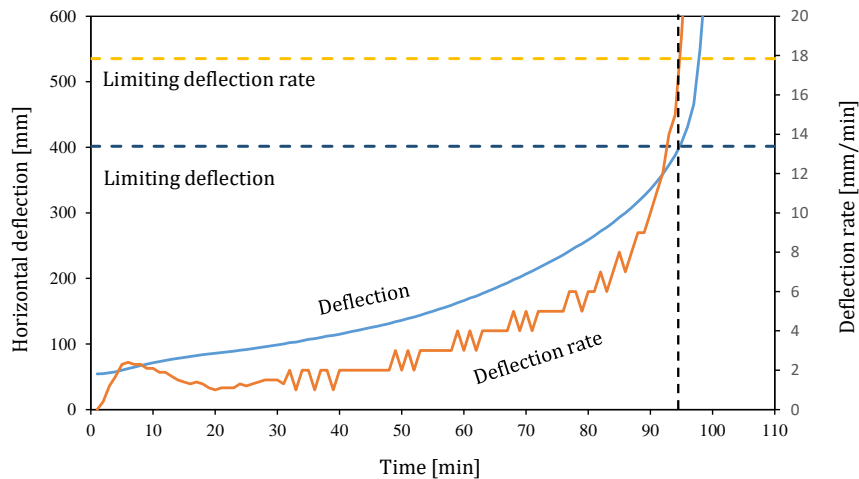


Figure 75 – Deflection and deflection rate vs. time obtained with SAFIR, considering the temperatures on the cross-section with only concrete, with limits for the loadbearing capacity according to the criteria in EN 1363-1 [6] for flexural loaded elements

Table 28 – Failure time, horizontal displacement and bending moment for Example 10, considering the temperatures on the cross-section with only concrete

Parameter			Reference	Calculated	Deviation	Limit	
			X	X'	$(X' - X) / X \cdot 100$		
					%	%	
Failure time t_u in min		min	93	95	2.15	± 3.00	
For $t = 90$ min	Temp. in rebars	corner	°C	502	484	-3.59	-
		Intermediate	°C	319	303	-5.02	-
	Hor. displacement ω_z at top of the column		mm	381	337	-11.55	± 15.00
	Moment $M_{E,fi,d}$ at bottom of the column		kN.m	75.5	71.7	-4.90	± 5.00

2.11. Example 11 – Composite column with concrete cores

2.11.1 *Keywords*

Fire resistance time, displacements, beam-column, composite section, ISO fire curve

2.11.2 *Objective*

Example 11 deals with a composite steel-concrete column with a partially encased steel section loaded with a vertical load, with an imperfect shape and subject to fire on all sides. The goal is to determine the failure time as well as the horizontal displacements for two intermediate times.

2.11.3 *Description of the problem*

The column with the characteristics defined in Figure 76 and Table 29 is analysed. It is considered that both ends are rotationally fixed in case of fire and that it has a geometrical imperfection with a parabolic shape with a maximum amplitude at mid-length equal to $l/1000$. In order to validate the results, the failure time for the member, as well as the horizontal displacement at mid-length for the time instants of 30 min and 60 min, are calculated and compared to the reference values presented in DIN EN1992-1-2 NA.

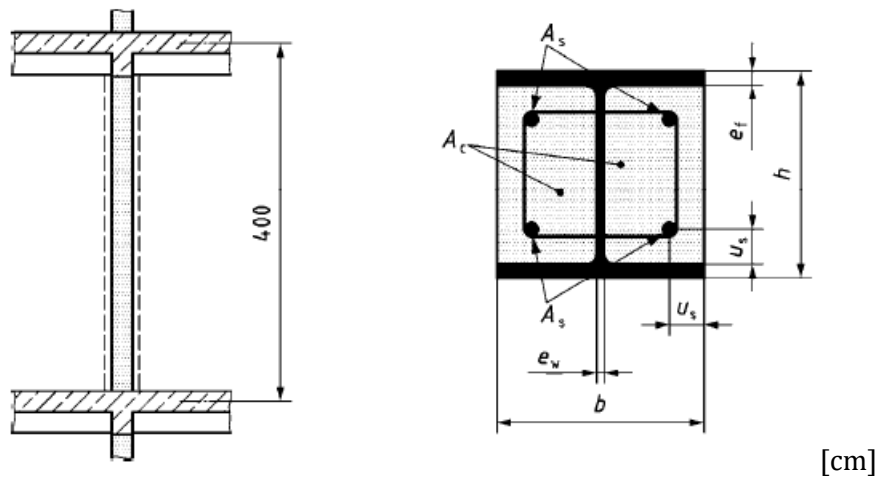


Figure 76 – Example 11: Cross-section and configuration of the composite column

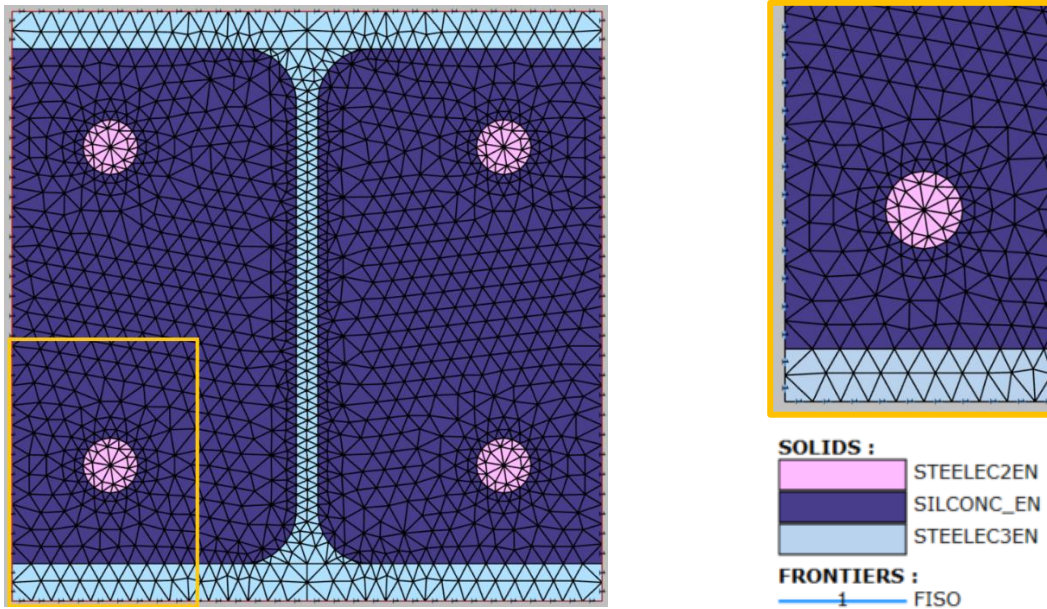
Table 29 – Dimensions, material properties and boundary conditions for Example 11

Properties			R90
Dimensions	l, b, h	mm	4000, 300, 300
	u_s	mm	50
	e_f	mm	19
	e_w	mm	11
Loads	$N_{E,fi,d,t}$	kN	-1700
Concrete C25/30 (3% humidity by mass)	$f_{ck}(20^\circ\text{C})$	N/mm ²	25
Steel B500	$f_{yk}(20^\circ\text{C})$	N/mm ²	500
Steel S235	$f_{ak}(20^\circ\text{C})$	N/mm ²	235
Stress-strain material law	Concrete ^a		EN 1994-1-2
	Rebars ^b		
	Structural steel		
Fire exposure	ISO 834 (four sides)		EN 1991-1-2
Heat transfer coefficient	α_c	W / (m ² .K)	25
Emissivity	ϵ_m		0.7
Thermal and physical material values	Concrete	$\lambda, \rho, c_p, \epsilon_{th,c}$	EN 1994-1-2
	Steel	$\lambda_a, \rho, c_a, \epsilon_{th,s}$	EN 1994-1-2
^a – with predominantly siliceous aggregates and density $\rho = 2400 \text{ kg/m}^3$			
^b – hot-rolled			

2.11.4 Models and results (see folder DIN11 4)

The cross-section was modelled with 2690 triangular finite elements, while the column was modelled in a 2D structural model with 20 BEAM elements of equal sizes (see Figure 77 and Figure 78).

The materials STEELEC2EN (defined as HOTROLLED and CLASS_B) and SILCONC_EN were used for the reinforced concrete part, whereas the I-profile was modelled with the material STEELEC3EN.



a) Overall view

b) Detail of one of the rebars

Figure 77 – Thermal model of the cross-section for Example 11

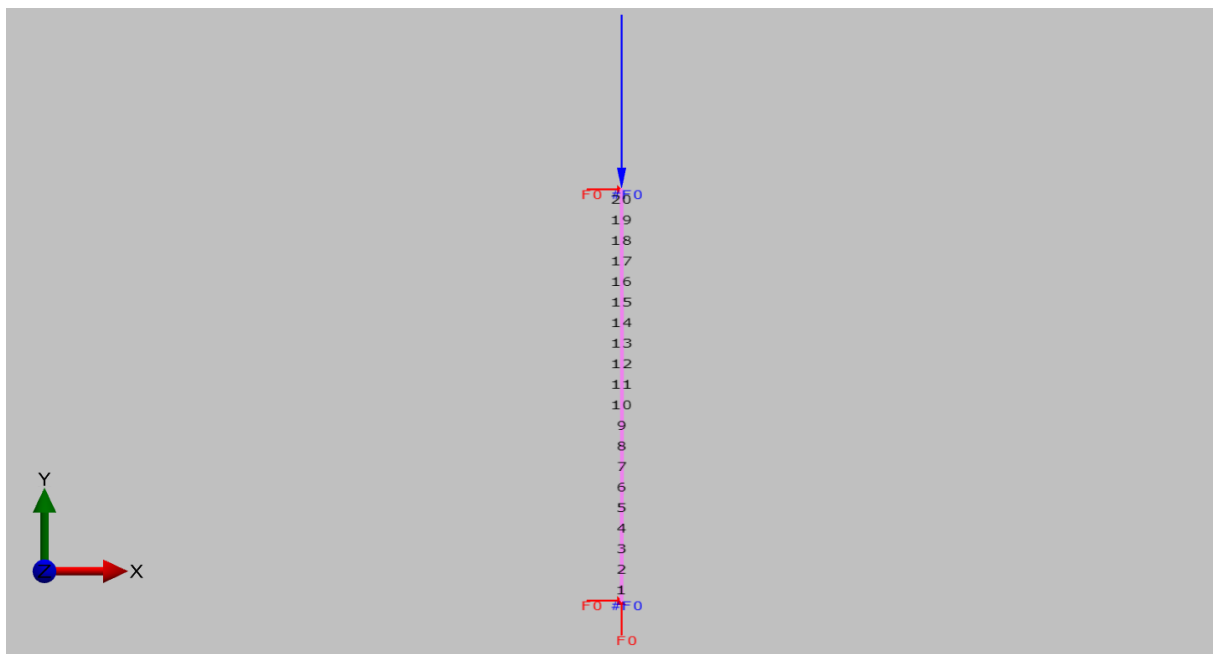


Figure 78 – Structural model of the column for Example 11 (20 BEAM elements with equal sizes)

The thermal model was defined with a PRECISION of 10E-3s and a time step of 10s. For the mechanical model it was defined a STATIC analysis with a PURE_NR method, with a PRECISION of 10E-3s, a COMEBACK of 1s and a time step of 60s.

The temperature distribution obtained by SAFIR for $t = 90$ min is presented in Figure 79.

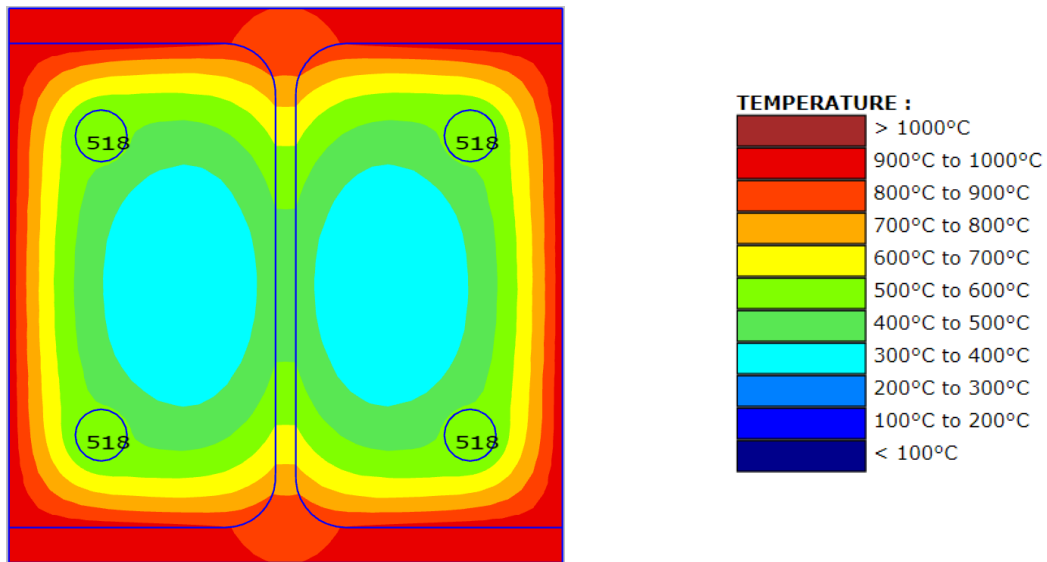


Figure 79 – Temperatures determined by SAFIR for Example 11, for $t = 90$ min

Figure 72 shows the evolution of the horizontal displacement at mid-length of the column. The horizontal displacement of the last converged time is 36 mm, corresponding to $l/111$.

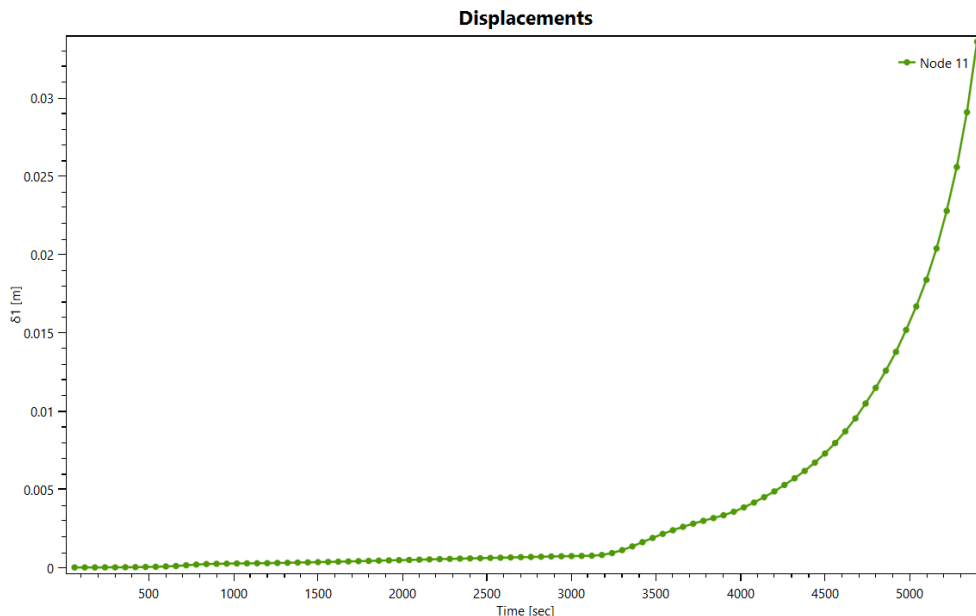


Figure 80 – Horizontal displacement vs. time for Example 11, for the node at mid-length of the column

The deviations from the DIN EN1992-1-2 NA can be found in Table 30. The failure time instant considered was the last converged time step.

Table 30 – Failure time and horizontal displacements for 30 min and 60 min for Example 11

Parameter			Reference	Calculated	Deviation	Limit
			X	X'	$(X' - X) / X \cdot 100$	
					%	
Failure time t_u	min		92	91	-1.08	± 5.00
Temperature for $t = 90$ min	rebars	°C	535	518	-3.18	-
	centre of profile	°C	447	460	2.91	-
Hor. displacement ω_z at mid-length	30 min	mm	4.4	4.45	1.14	± 5.00
	60 min	mm	5.5	6.18	12.36	± 5.00

2.11.5 Discussion and conclusions

As in the previous examples, the temperature determined by SAFIR for the rebars is lower than the one provided by the DIN. In this case, the temperature determined in the rebars is 3.18% less than the reference value. On the contrary, the temperature determined at the centre of the profile was 2.91% higher than the one in DIN. There is no apparent explanation for this, but it has been observed that the software Infograph (see [7]) obtain values (523°C for the rebars and 469°C for the centre of the profile) that are closer to the values of SAFIR than to the reference values.

As for the fire resistance time, a value slightly inferior (-1.08%) to the one presented in the DIN was obtained, considering the last converged time step as the time of failure of the column. None of the limits for the EN1363-1 criteria, neither for flexural nor for vertically loaded members, were reached (nor close to be reached) for this case and it is therefore not possible to apply these criteria for the determination of the time of failure of the column.

Regarding the horizontal displacements at mid-length for $t = 30$ min and $t = 60$ min, it is important to note that the displacements indicated in DIN appear to be given by reference to the initial straight position, not considering the imperfection applied, and hence the values present in Table 30 include the displacement calculated by SAFIR plus the 4mm of initial imperfection ($l/1000$). When this initial imperfection is taken into account, the value determined by SAFIR after 30 minutes lies well inside the interval allowed by the DIN, although the same doesn't happen after 60 minutes of fire, missing the interval by 7.36%.

3. General conclusions

It can be observed that the majority of the results analysed fell well inside the boundaries stipulated in the Annex CC of the DIN EN1992-1-2 NA, and possible justifications were provided when that was not the case. Different behaviours like the heat-transfer (heating and cooling) in

the thermal analyses or the temperature-dependent elongations and stresses in the mechanical analyses are therefore validated by the results presented in this document.

Most of the uncertainties and doubts are about the reference values provided by the DIN for the last 4 cases, given that the latter are cases in which the reference solution provided by the DIN is not theoretical, but instead comes from simulation results with other software. Even though the software used to calculate the reference values are referred to as 'approved tools', there lacks a description about these software, the modelling assumptions, and the failure criteria, which is needed to rigorously compare these reference results with results obtained from another software. It was not possible to find detailed reports on those analyses, and therefore it was not possible to point out what may be the exact causes for the differences found between the results determined by SAFIR and those found in the DIN for those 4 cases.

When comparison was possible between the results provided by SAFIR and those provided by other software, the results of SAFIR were very similar to the results of the other software.

4. References

[1] Franssen J. M., Gernay T. (2017), "Modeling structures in fire with SAFIR®: Theoretical background and capabilities", *Journal of Structural Fire Engineering*, Vol. 8, No 3, 300-323. <https://doi.org/10.1108/JSFE-07-2016-0010>

[2] DIN EN 1991-1-2/NA (2010), "National Annex - National determined parameter – Eurocode 1: Actions on structures – Part 1-2: General actions – Actions on structures exposed to fire", Deutsche Norm.

[3] CEN (2005), EN 1992-1-2 "Eurocode 2: Design of concrete structures – Part 1-2 – General rules – Structural fire design", European Committee for Standardisation, Brussels.

[4] CEN (2005), EN 1993-1-2 "Eurocode 3: Design of steel structures – Part 1-2 – General rules – Structural fire design", European Committee for Standardisation, Brussels.

[5] CEN (2005), EN 1994-1-2 "Eurocode 4: Design of composite steel-concrete structures – Part 1-2 – General rules – Structural fire design", European Committee for Standardisation, Brussels.

[6] CEN (2012), EN 1363-1 "Fire resistance tests – Part 1: General requirements", European Committee for Standardisation, Brussels.

[7] Infograph (2015), "Prüfung und validierung von rechenprogrammen für brandschutznachweise mittels allgemeiner rechenverfahren,", http://download.infograph.de/de/validierung_brand.pdf (url last consulted on 25/09/2017).

[8] FRILO (2017), “Analyses on reinforced concrete section”
http://www.frilo.eu/tl_files/frilo/pdf/en/pdf_doku/Analyses%20on%20Reinforced%20Concrete%20Cross%20Sections.pdf (url last consulted on 25/09/2017).

[9] COST report (2014), “Benchmark studies - Verification of numerical models in fire engineering”, ISBN: 978-80-01-05442-0, Czech Technical University in Prague, 23-29.

[10] Hosser D., Richter E., Zehfuß J., “Erarbeitung von Nationalen Anwendungsrichtlinien für rechnerische Nachweise nach den Brandschutzteilen der Eurocodes 2 – 5”, Abschlussbericht im Auftrag des Bundesministeriums für Raumordnung, Bauwesen und Städtebau (Az. RS III 4 – 67 41 – 97.120). Institut für Baustoffe, Massivbau und Brandschutz (iBMB), Braunschweig, 1999 (in German).

[11] Mbaec (2014), “Validierung gemäß DIN EN 1991-1-2 / NA:2015-09”,
https://www.mbaec.de/fileadmin/Datenblaetter/U412de_Validierung.pdf (url last consulted on 25/09/2017)